A&A manuscript no.
(will be inserted by hand later)

Your thesaurus codes are:
06 (02.19.1; 08.03.4; 08.06.2; 09.08.1; 09.10.1; 13.09.6)

ASTRONOMY AND ASTROPHYSICS
August 29, 2000

ISO Spectroscopy of PDRs and Shocks in Star Forming Regions ⋆

M.E. van den Ancker[1,2], A.G.G.M. Tielens[3,4], and P.R. Wesselius[4]

[1] Astronomical Institute "Anton Pannekoek", University of Amsterdam, Kruislaan 403, NL–1098 SJ Amsterdam, The Netherlands
[2] Harvard-Smithsonian Center for Astrophysics, 60 Garden Street, MS 42, Cambridge MA 02138, USA
[3] Kapteyn Astronomical Institute, Groningen University, P.O. Box 800, NL–9700 AV Groningen, The Netherlands
[4] SRON, P.O. Box 800, NL–9700 AV Groningen, The Netherlands

Received <date>; accepted <date>

Abstract. We present the results of ISO SWS and LWS grating scans of pure rotational lines of H_2, as well as the infrared fine structure lines of [C II], [O I], [S I], [Si II], [Fe I] and [Fe II] towards galactic star forming regions. We find that intense H_2 emission is only observed in the vicinity of stars with spectral type earlier than B4 or in the neighbourhood of embedded YSOs associated with outflows. We interpret these lines as arising in either a photo-dissociation region (PDR) near the early-type stars, or a shock caused by the interaction of an outflow with the surrounding molecular cloud material. Molecular hydrogen excitation temperatures and fine structure line intensities were compared with those predicted by theoretical models for PDRs and dissociative and non-dissociative shocks and to those observed towards regions known to contain PDRs and shocks. It is shown that both shocks and PDRs show a warm and hot component in H_2. The observed temperatures of the warm component appear in general too high to be explained by current dissociative shock models. We find that the mere detection of [S I] 25.2 μm emission with ISO is an unambiguous sign of the presence of shocked gas. Strong [C II] 157.7 μm can only be due to a PDR. An evolutionary scenario is suggested in which the circumstellar material around a young star changes from being heated mechanically by shocks into heated by radiation from the central star through a PDR as the star clears its surroundings.

Key words: Shock waves – Circumstellar matter – Stars: Formation – H II regions – ISM: Jets and outflows – Infrared: Stars

1. Introduction

The infrared emission-line spectrum of Young Stellar Objects (YSOs) is dominated by the interaction of the central object with the remnants of the clouds from which it formed. The intense UV radiation generated by accretion as well as by the central star itself causes dissociation of molecular material close to the YSO and ionizes much of the atomic material, giving rise to typical nebular and recombination lines. The strong stellar wind, often collimated into a bipolar outflow, will cause a shock wave as it hits the surrounding molecular cloud, heating the post-shock gas sufficiently to cause strong molecular and ionic emission.

Neutral clouds irradiated by far-ultraviolet (FUV) photons are known as photodissociation regions (PDRs; see Hollenbach & Tielens 1999 for a comprehensive review). In these regions, heating of the gas occurs by collisions of photoelectrically ejected electrons from grain surfaces. Cooling of the gas occurs mainly through emission in atomic fine-structure and molecular lines, reaching intensities that should be easily observable in a wide range of astronomical objects. The gas in the surface regions of these PDRs reaches temperatures of typically 500 K (e.g. Tielens & Hollenbach 1985), making it possible to collisionally excite the low-lying pure rotational levels of molecular hydrogen, provided that the region has a sufficient density and incident FUV flux. Since the lowest ro-vibrational lines of H_2 have energy levels of the order of 5000 K, only these low-lying pure rotational H_2 lines, hard to observe from the ground, can reliable probe the physical conditions of the dominant species and thus provide us with detailed information of the physical conditions occurring in the PDR.

The physical situation in shock waves is quite distinct: here the molecular gas is heated by compression of a supersonic wave moving through the gas. Shocks are usually divided into two distinct categories: J- or Jump-shocks, and C- or Continuous-shocks. In the J-shocks viscous heating of the neutrals occurs in a thin shock front in which radiative cooling is insignificant, and the post-shock gas is heated to several times 10^4 degrees (e.g. Hollenbach & McKee 1989), dissociating all molecular material. In these J-shocks, the physical conditions (density, temperature) change from their pre- to post-shock values within one mean free path, causing an apparent discontinuity. Cooling of the post-shock gas occurs trough atomic fine-structure lines.

C-shocks are magnetized, non-dissociative shocks in which ions and the magnetic field are compressed ahead of the shock front and are able to heat the neutral gas (containing only a trace fraction of ions) to a few thousand degrees. In C-shocks the physical conditions change more gradually from their pre- to post-shock values and cooling is mainly through radiation

Send offprint requests to: M.E. van den Ancker (mario@astro.uva.nl)
⋆ Based on observations with ISO, an ESA project with instruments funded by ESA Member States (especially the PI countries: France, Germany, the Netherlands and the United Kingdom) and with the participation of ISAS and NASA.

Table 1. Properties of programme stars.

Source	α (2000)	δ (2000)	Region	d [pc]	Ref.	Sp. Type	$T_{\rm eff}$ [K]	Ref.	Outflow	A_V [$^{\rm m}$]	$\log L/L_\odot$	$M_\star$ [$M_\odot$]	Age [yr]
AFGL 490	03 27 38.6	+58 47 00	Cam OB1	900	(1)	B1–6e	18000	(13)	√	≈ 31	3.57	≈ 8	–
IRAS03260+3111	03 29 10.4	+31 21 58	NGC 1333	350	(2)		12000	(14)	–	≈ 20	2.45	≈ 4	–
L1489 IRS	04 04 43.0	+26 18 58	L1491	140	(3)	$>$ Ke	4000	(15)	√	≈ 20	0.60	< 2	–
L1551 IRS5	04 31 34.0	+18 08 04	Tau R2	140	(3)	G–Ke	5500	(15)	√	≈ 19	1.37	≈ 3	–
IRAS12496−7650	12 53 16.0	−77 07 02	Cha II	180	(4)	Ae	8600	(16)	√	≈ 14	1.68	≈ 2.5	–
GGD 27-ILL	18 19 12.0	−20 47 31	IC 1318	1700	(5)	B1	25000	(17)	√	≈ 20	4.29	≈ 14	–
LkHα 225	20 20 30.4	+41 21 27	Cyg R1	1000	(6)	A–Fe	9000	(18)	√	≈ 15	3.21	≈ 7	–
S106 IRS4	20 27 26.6	+37 22 48	Cyg OB2	1200	(7)	O6–O8e	37000	(19)	–	≈ 14	4.62	≈ 20	–
AFGL 2591	20 29 24.6	+40 11 19	Cyg X	1700	(8)	$<$ O8	40000	(20)	√	≈ 30	4.78	≈ 25	–
Cep A East	22 56 18.6	+62 02 00	Cep OB3	690	(9)	B:	22000	(20)	√	≈ 62	3.65	≈ 9	–
Elias 3-1	04 18 40.5	+28 19 17	L1495	140	(3)	A6:e	8000	(21)	–	7.83	1.32	2.0	3×10^6
T Tau	04 21 59.1	+19 32 06	Tau R2	140	(3)	K0–1e	5200	(22)	√	1.39	1.22	2.5	$< 10^6$
HD 97048	11 08 04.6	−77 39 17	Ced 111	180	(10)	B9.5Ve	10000	(23)	–	1.27	1.50	2.5	$\geq 3 \times 10^6$
HD 97300	11 09 50.6	−76 36 47	Ced 112	190	(10)	B9V	10500	(24)	–	1.33	1.42	2.4	$\geq 3 \times 10^6$
HR 5999	16 08 34.2	−39 06 18	Lupus 3	210	(10)	A5–7IIIe	7900	(25)	–	0.47	1.96	3.2	5×10^5
R CrA	19 01 53.9	−36 57 10	NGC 6729	130	(11)	A1–F7ev	8600	(10)	√	2.26	1.98	3.0	1×10^6
T CrA	19 01 58.8	−36 57 49	NGC 6729	130	(11)	F0e	7200	(26)	√	1.64	0.88	1.5	1×10^7
WW Vul	19 25 58.6	+21 12 31	Vul R1	440	(12)	A4IV–Ve	8400	(27)	–	0.96	1.33	2.0	5×10^6
BD+40°4124	20 20 28.3	+41 21 51	Cyg R1	1000	(6)	B2Ve	22000	(17)	–	3.01	3.16	7.0	$\geq 10^5$
LkHα 224	20 20 29.2	+41 21 27	Cyg R1	1000	(6)	A7e	7900	(28)	–	2.98	2.27	4.0	1×10^5
HD 200775	21 01 36.8	+68 09 49	NGC 7023	430	(10)	B2.5IVe	20400	(29)	√	1.92	3.36	9.0	2×10^7

References to Table 1: (1) Harvey et al. (1979); (2) Herbig & Jones (1983); (3) Kenyon et al. (1994); (4) Whittet et al. (1997); (5) Rodríguez et al. (1980); (6) Shevchenko et al. (1991); (7) Rayner (1994); (8) Dame & Thaddeus (1985); (9) Mel'nikov et al. (1995); (10) van den Ancker et al. (1997, 1998); (11) Marraco & Rydgren (1981); (12) Voshchinnikov (1981); (13) Snell et al. (1984); (14) This paper; (15) Kenyon et al. (1998); (16) Hughes et al. (1991); (17) Yamashita et al. (1987); (18) Hillenbrand et al. (1995); (19) van den Ancker et al. (2000b); (20) Lada et al. (1984); (21) Zinnecker & Preibisch (1994); (22) Kenyon & Hartmann (1995); (23) Whittet et al. (1987); (24) Rydgren (1980); (25) Tjin A Djie et al. (1989); (26) Finkenzeller & Mundt (1984); (27) Gray & Corbally (1998); (28) van den Ancker et al. (2000a); (29) Rogers et al. (1995).

from molecular material (e.g. Kaufman & Neufeld 1996). If the temperatures in a C-shock become sufficiently high to start to dissociate molecules, the cooling through the molecular lines goes down, and the shock temperature increases until it turns into a J-shock. Shocks with a velocity larger than 40 km s^{-1} are usually J-shocks, whereas slower shocks are usually of C-type (Chernoff et al. 1982).

In this paper we will study the infrared emission-line spectra of a sample of YSOs observed with the *Infrared Space Observatory* (ISO; Kessler et al. 1996). In order to interpret our observations as arising in either a PDR, C-Shock or J-shock, we compare measured line intensities with those predicted by theoretical models of such regions. Since the regions surrounding our target sources are often highly confused, and the applicability of the simplified models to a complex physical situation is by no means sure, we will also compare our new ISO observations with those of relatively clean regions known to contain a shock or a PDR. We will show that the distinction between a shock and a PDR spectrum can be made with relative ease and the infrared lines are a good diagnostic tool for constraining the physical conditions in the material surrounding YSOs.

2. Sample selection

Young stellar objects are commonly divided into classes depending on their energy distribution. Class I YSOs are heavily embedded, optically invisible, but usually infrared bright objects. Class II YSOs are already optically visible, but also still show excess infrared emission above photospheric levels due to dust, heated by the central star, in the direct circumstellar environment. Intermediate-mass (2–10 M$_\odot$) Class II YSOs are usually referred to as Herbig Ae/Be stars, whereas their lower mass counterparts are the T Tauri stars. In the remainder of this paper we will study the infrared emission line spectra in the vicinity of a sample of 10 Class I YSOs and 11 Class II sources. They are listed in Table 1. Because of the brightness limitations imposed by the instruments used, the sample is biased towards infrared bright objects, either because they are inherently anomalously luminous in the infrared or because they are located relatively nearby.

To understand the occurrence of infrared emission lines due to PDRs or shocks in the vicinity of the stars in our sample, it is useful to derive their basic properties in a consistent way. We have therefore made new estimates of the bolometric luminos-

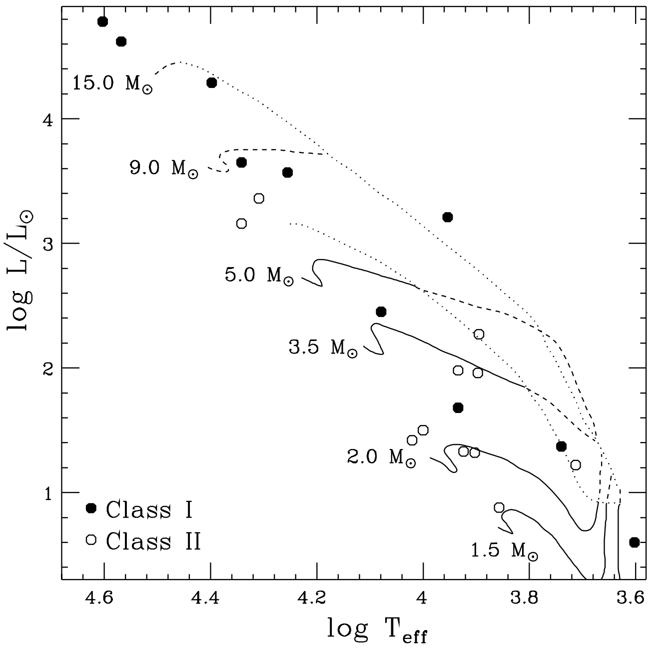

Fig. 1. Hertzsprung-Russell diagram for the YSOs included in this study. Filled and open plot symbols indicate Class I and II sources, respectively. Also shown are theoretical PMS evolutionary tracks (solid/dashed lines) and the birthlines for 10^{-4} (upper dotted line) and 10^{-5} $M_\odot$ yr^{-1} (lower dotted line) by Palla & Stahler (1993).

ity of each source by constructing spectral energy distributions (SEDs), using ultraviolet to submm data compiled from literature. A fit consisting of the sum of a reddened Kurucz (1991) model for the stellar photosphere and a spline fitted to the excesses in the infrared to submm range, extrapolated to infinity by a blackbody curve, was made to the energy distribution for each source. Total bolometric luminosities were then determined by computing $4\pi d^2 \int F_\lambda \mathrm{d}\lambda$, with d the distance to the source and F_λ the SED fit. The results of this procedure, as well as the distances and effective temperatures used, are listed in Table 1. For the extincted sources the resulting values of $L_{\rm bol}$ do not depend on the adopted value of $T_{\rm eff}$.

From the results listed in Table 1 we have created the Hertzsprung-Russell diagram (HRD) shown in Fig. 1. In this figure, we also have plotted the pre-main sequence evolutionary tracks and the birthline by Palla & Stahler (1993). By comparing the location of a source in the HRD with these computations, we can determine stellar masses and ages for pre-main sequence stars. For single Class II sources the required parameters (luminosity and temperature) can be determined fairly accurately. For the Class I sources, the temperature is usually not well determined, but since the luminosity of an intermediate-mass star stays relatively constant during its contraction to the zero-age main sequence, the evolutionary tracks can still be used to estimate its mass. Resulting stellar masses and ages are also listed in Table 1.

Table 2. Log of ISO observations of programme stars.

Object	AOT	Rev.	Date	JD−2450000
AFGL 490	LWS 01	623	31/07/1997	660.879
	SWS 01	640	17/08/1997	6780200
	SWS 02	863	27/03/1998	899.939
IRAS03260+3111	SWS 01	659	05/09/1997	696.880
	LWS 01	848	12/03/1998	884.909
L1489 IRS	SWS 02	654	31/08/1997	691.635
L1551 IRS5	SWS 01	660	06/09/1997	697.769
	SWS 02	668	14/09/1997	705.561
	LWS 01	668	14/09/1997	705.571
IRAS12496−7650	LWS 01	115	11/03/1996	153.678
	SWS 02	141	06/04/1996	179.909
	SWS 01	233	06/07/1996	271.331
GGD27-ILL	LWS 01	148	13/04/1996	187.161
	SWS 02	149	14/04/1996	187.595
	SWS 01	149	14/04/1996	187.621
LkHα 225	SWS 02	142	07/04/1996	180.996
	LWS 01	142	07/04/1996	181.017
	SWS 02	355	05/11/1996	393.306
	SWS 01	858	22/03/1998	894.889
S106 IRS4	SWS 02	134	30/03/1996	172.705
	LWS 01	134	30/03/1996	172.726
	SWS 01	335	17/10/1996	373.740
AFGL 2591	SWS 02	134	30/03/1996	172.577
	LWS 01	142	07/04/1996	180.737
	SWS 01	357	07/11/1196	395.296
Cep A East	SWS 02	220	23/06/1996	258.463
	LWS 01	566	04/06/1997	603.681
	SWS 02	566	04/06/1997	603.706
	SWS 01	843	07/03/1998	880.050
Elias 3-1	SWS 02	667	13/09/1997	704.605
	SWS 01	673	19/09/1997	710.564
T Tau	LWS 01	672	18/09/1997	709.675
	SWS 01	680	25/09/1997	717.411
	SWS 02	681	27/09/1997	718.778
	SWS 02	861	25/03/1998	897.973
HD 97048	SWS 01	141	06/04/1996	179.947
	LWS 01	261	04/08/1996	299.565
HD 97300	SWS 02	141	06/04/1996	179.826
HR 5999	SWS 01	289	01/09/1996	327.627
	SWS 02	289	01/09/1996	327.669
R CrA	LWS 01	495	25/03/1997	533.284
	SWS 02	704	19/10/1997	741.322
	SWS 01	704	19/10/1997	741.353
T CrA	SWS 02	141	06/04/1996	179.738
	SWS 01	689	04/10/1997	726.278
WW Vul	SWS 01	176	11/05/1996	214.507
	SWS 02	176	11/05/1996	214.541
	SWS 02	865	29/03/1998	901.889
BD+40°4124	SWS 02	142	07/04/1996	181.037
	SWS 02	159	24/04/1996	197.635
	SWS 01	355	05/11/1996	393.283
	LWS 01	768	23/12/1997	805.525
LkHα 224	SWS 02	142	07/04/1996	180.960
	SWS 01	858	22/03/1998	894.920
HD 200775	SWS 02	143	08/04/1996	182.108
	SWS 01	339	21/10/1996	377.670
	LWS 01	339	21/10/1996	377.695

3. Observations

As part of the ISO Guaranteed Time programme on YSOs ("YSOAEBE", P.I. P.R. Wesselius), we obtained spectroscopic data centered on the positions of the 21 young stellar objects listed in Table 1. Selected infrared transitions of H_2, [Fe I], [Fe II], [S I], [Si II], [O I] and [C II] were scanned with the Short (SWS: 2.4–45 μm; de Graauw et al. 1996) and Long Wavelength (LWS: 43–197 μm; Clegg et al. 1996) Spectrometers on board ISO. Most of the lines in the SWS wavelength range were scanned with the full grating resolution ("AOT S02"), although in some objects some were taken from lower resolution full grating scans ("AOT S01"). All lines in the LWS wavelength range were obtained from LWS full grating scans ("AOT L01"). After the release of all ISO data to the public domain, we inspected the ISO data archives for any additional spectroscopy on our 21 targets and also included those in our data-set. A full log of the ISO observations used in this study is given in Table 2.

Data were reduced in a standard fashion using calibration files corresponding to ISO off-line processing software (OLP) version 7.0, after which they were corrected for remaining fringing and glitches. To increase the S/N in the final spectra, detectors were aligned and statistical outliers were removed, after which the spectra were rebinned to a lower spectral resolution (SWS) or simply averaged (LWS).

Scanned lines and measured line fluxes for the detected lines or upper limits (total flux for line with peak flux 3σ) for the undetected lines are listed in Table 3. For the sources in which AOt S01 data is available, we also report the flux in the 6.2 μm UIR band. In a number of sources the H_2 0–0 S(2) line was not detected because of strong fringing of the continuum in this part of the spectrum, either due to the continuum source being spatially extended, or due to the continuum source not being in the center of the beam. The H_2 0–0 S(6) line has a wavelength that puts it the middle of the H_2O ν_2 absorption band, also hindering its detection in some sources (e.g. LkHα 225; van den Ancker et al. 2000a).

Accuracies of the absolute flux calibration in the SWS spectra range from 7% in the short-wavelength (< 4.10 μm) part to $\approx 30\%$ in the long wavelength (> 29 μm) part (Leech et al. 1997). The LWS absolute flux calibration is expected to be accurate at the 7% level (Trams et al. 1997). The errors listed in Table 3 include both the error in the line flux measurement itself and this absolute error. Note that the applied flux calibration is based on the assumption that we are looking at a point source. For an extended source, the diffraction losses will be underestimated and, in particular at the long-wavelength part of the LWS, these corrections will exceed the quoted uncertainty.

4. Molecular hydrogen emission

From the H_2 line fluxes $I(J)$ listed in Table 3 it is possible to calculate the apparent column densities of molecular hydrogen in the upper J levels, averaged over the SWS beam, $N(J)$, using $N(J) = \frac{4\pi I(J)}{A}\frac{\lambda}{hc}$, with λ the wavelength, h Planck's constant and c the speed of light. The transition probabilities A were taken from Turner et al. (1977). Line fluxes were corrected for extinction using the average interstellar extinction law by Fluks et al. (1994) using the values compiled in Table 1.

A useful representation of the H_2 data is then to plot the log of $N(\mathrm{J})/\mathrm{g}$, the apparent column density for a given J upper level divided by the statistical weight, versus the energy of the upper level. The resulting excitation diagrams are shown in Fig. 2. For a Boltzmann distribution, the points in Fig. 2 should form a nearly straight line. The slope of this line is inversely proportional to the excitation temperature, while the intercept is a measure of the total column density of warm gas. Since the A coefficients for the H_2 lines are quite small, these lines are optically thin and, because the critical densities are low, the excitation temperature will be close to the kinetic temperature of the gas.

The statistical weight g is a combination of the rotational and nuclear spin components. For this, we have assumed the high temperature equilibrium relative abundances of 3:1 for the ortho and para forms of H_2 (Burton et al. 1992a). From Fig. 2 it is apparent that for most sources, the H_2 points below 5000 K do indeed form a straight line in the excitation diagram. The fact that the points for ortho and para H_2 lie on the same line proves that our assumption on their relative abundances is correct.

Using the formula by Parmar et al. (1991) and the rotational constants by Dabrowski (1984), we have fitted Boltzmann distributions to the low-lying pure rotational lines. For a number of sources, the pure rotational lines at the higher energy levels can be seen to deviate strongly from this fit. In these cases, we have attempted to characterize this behaviour by fitting a second Boltzmann distribution to the higher energy level populations. The resulting excitation temperatures and derived column and mass of molecular hydrogen are listed in Table 5.

In Fig. 2 we also show similar plots for six regions which have been quoted in literature as prime examples of shock- and PDR emission, peak 1 of the shocked H_2 emission in the Orion BN/KL region (Hasegawa et al. 1987; Brand et al. 1988; Parmar et al. 1994; Rosenthal et al. 2000), the shock in the old supernova remnant IC 443 (Burton et al. 1989; Richter et al. 1995a, 1995b; Oliva et al. 1999a; Cesarsky et al. 1999), the X-ray irradiated shock in the young supernova remnant RCW 103 (Oliva et al. 1990, 1999b), the Orion bar PDR (Burton et al. 1990a; Parmar et al. 1991; Marconi et al. 1998), the NGC 2023 PDR (Hasegawa et al. 1987; Burton et al. 1992b; Steiman-Cameron et al. 1997) and the PDR S140 (Timmermann et al. 1996). The ground-based observations of these regions reveal spatial structure in the derived temperature on a scale which is small compared to the ISO SWS beam. Basic parameters for these regions are listed in Table 4. As can be seen from Fig. 2, the excitation diagrams of these template regions show in general the warm and hot component also visible in some of our ISO sources. The results of the Boltzmann distribution fits are again given in Table 5.

Employing predictions of H_2 emission from PDR, J-shock and C-shock models by Burton et al. (1992a), Hollenbach & McKee (1989) and Kaufman & Neufeld (1996), we determined the excitation temperature $T_{\rm rot}$ from the low-lying (from S(1) to S(5)) pure rotational levels from these models as a function of density n and either incident FUV flux G (in units of the average interstellar FUV field $G_0 = 1.2 \times 10^{-4}$ erg cm^{-2} s^{-1} sr^{-1}; Habing 1968) or shock velocity v_s in an identical way as was done for the observations. For PDRs, the total infrared flux F_{IR} is expected to be directly correlated to G by the relation $G = 0.5\ F_{IR}/\Omega^2$, with Ω the spatial extent of the PDR. We have computed F_{IR} for all our sources by the same procedure as was used to compute the bolometric luminosity in Sect. 2, but in this case only use the excess above the reddened Kurucz model to integrate F_λ. From these values of F_{IR} we then computed G,

Table 3. Observed and extinction-corrected line fluxes (in 10^{-16} W m^{-2}).

Line	λ	Beam	AFGL 490		IRAS03260+3111		L1489 IRS		L1551-IRS5		IRAS12496−7650	
	[μm]	[10^{-8} sr]	Obs.	Ext. corr.	Obs.	Ext. Corr.	Obs.	Ext. Corr.	Obs.	Ext. Corr.	Obs.	Ext. Corr.
H_2 0–0 S(0)	28.2188	1.64	< 39.9	< 40.3	< 5.65	< 5.71	< 5.59	< 5.64	< 20.6	< 20.8	< 7.89	< 7.97
H_2 0–0 S(1)	17.0348	1.15	< 16.9	< 17.2	16.6±3.6	16.9±3.6	< 1.07	< 1.09	< 1.94	< 1.97	1.11±0.36	1.13±0.37
H_2 0–0 S(2)	12.2786	1.15	< 52.3	< 53.5	33.0±9.4	33.7±9.7	< 21.1	< 21.7	< 16.2	< 16.6	< 20.1	< 20.5
H_2 0–0 S(3)	9.6649	0.85	3.77±1.24	3.99±1.32	21.7±5.5	22.9±5.8	< 2.03	< 2.15	< 1.97	< 2.08	2.51±0.83	2.70±0.89
H_2 0–0 S(4)	8.0251	0.85	< 15.9	< 16.2	10.2±2.7	10.4±2.8	< 2.81	< 2.87	< 3.04	< 3.10	< 2.96	< 3.02
H_2 0–0 S(5)	6.9095	0.85	9.62±2.43	9.72±2.45	20.1±3.8	20.4±3.8	< 2.75	< 2.78	< 2.77	< 2.80	< 4.96	< 5.01
H_2 0–0 S(6)	6.1086	0.85	< 23.0	< 23.2	< 50.2	< 50.8	–	–	< 13.9	< 14.1	< 12.0	< 12.1
H_2 0–0 S(7)	5.5112	0.85	< 30.7	< 31.1	< 17.3	< 17.6	< 13.5	< 13.7	< 10.0	< 10.1	< 13.0	< 13.2
H_2 0–0 S(8)	5.0531	0.85	< 23.1	< 23.3	< 7.70	< 7.82	–	–	< 4.78	< 4.85	< 22.5	< 22.7
H_2 0–0 S(9)	4.6946	0.85	< 27.8	< 28.2	< 8.67	< 8.82	–	–	< 6.93	< 7.03	< 59.4	< 60.5
H_2 0–0 S(10)	4.4099	0.85	< 9.50	< 9.69	< 5.07	< 5.16	–	–	< 6.78	< 6.92	< 12.8	< 13.1
H_2 0–0 S(11)	4.1813	0.85	< 10.7	< 10.9	< 11.0	< 11.2	–	–	< 13.9	< 14.2	< 7.56	< 7.72
[Fe I] ($^5D_4$–$^5D_3$)	24.0424	1.15	< 24.2	< 24.6	< 5.06	< 5.13	–	–	< 3.16	< 3.20	< 1.47	< 1.49
[Fe I] ($^5D_3$–$^5D_2$)	34.7135	2.01	< 7.25	< 7.30	< 12.4	< 12.5	< 5.72	< 5.76	< 7.22	< 7.27	< 4.58	< 4.62
[Fe II] ($^4F_{9/2}$–$^4F_{7/2}$)	17.9363	1.15	< 3.44	< 3.51	< 2.36	< 2.41	–	–	5.43±1.81	5.54±1.85	0.62±0.20	0.63±0.21
[Fe II] ($^6D_{9/2}$–$^6D_{7/2}$)	25.9882	1.15	< 24.3	< 24.6	< 3.31	< 3.35	–	–	12.6±4.2	12.8±4.2	0.75±0.25	0.76±0.25
[Fe II] ($^6D_{7/2}$–$^6D_{5/2}$)	35.3491	2.01	< 7.63	< 7.69	< 7.30	< 7.35	–	–	< 26.4	< 26.5	< 5.15	< 5.18
[S I] ($^3P_2$–$^3P_1$)	25.2490	1.15	< 9.91	< 10.0	< 6.97	< 7.06	< 2.05	< 2.08	< 8.26	< 8.37	< 2.56	< 2.59
[Si II] ($^2P_{1/2}$–$^2P_{3/2}$)	34.8152	2.01	5.64±1.86	5.68±1.87	27.2±9.0	27.4±9.1	< 7.20	< 7.26	20.1±6.6	20.3±6.7	5.37±1.77	5.41±1.79
[O I] ($^3P_2$–$^3P_1$)	63.1850	16.3	222.0±15.5	222.7±15.6	1083±76	1086±76	–	–	111.2±7.8	111.6±7.8	43.0±3.0	43.1±3.0
[O I] ($^3P_1$–$^3P_0$)	145.535	8.82	26.9±4.6	26.9±4.6	190.8±13.4	190.9±13.4	–	–	< 18.7	< 18.7	3.10±0.80	3.10±0.80
[C II] ($^2P_{1/2}$–$^2P_{3/2}$)	157.741	11.6	62.1±5.5	62.2±5.5	323.1±22.6	323.2±22.6	–	–	< 19.1	< 19.1	4.00±1.00	4.01±1.00
UIR (C–C stretch)	6.22	0.85	< 484	< 488	1327±99	1359±102	–	–	< 691	< 698	< 416	< 420

Line	λ	Beam	GGD27-ILL		LkHα 225		S106 IRS4		AFGL 2591		Cep A East	
	[μm]	[10^{-8} sr]	Obs.	Ext. corr.	Obs.	Ext. Corr.	Obs.	Ext. Corr.	Obs.	Ext. Corr.	Obs.	Ext. Corr.
H_2 0–0 S(0)	28.2188	1.64	< 12.1	< 12.3	< 13.8	< 14.3	< 15.8	< 16.7	< 124.2	< 125.5	< 36.2	< 36.9
H_2 0–0 S(1)	17.0348	1.15	5.57±1.84	5.68±1.87	7.76±2.56	8.23±2.72	5.76±1.75	7.54±2.29	17.9±4.7	18.3±4.8	2.73±0.90	2.84±0.94
H_2 0–0 S(2)	12.2786	1.15	< 41.5	< 42.5	21.8±7.2	23.3±7.7	11.8±4.9	16.1±6.6	< 189.9	< 194.3	12.7±4.2	13.3±4.4
H_2 0–0 S(3)	9.6649	0.85	5.63±1.86	5.95±1.96	28.0±7.3	33.1±8.7	11.9±3.9	25.5±8.4	13.5±3.7	14.3±3.9	9.02±2.98	10.1±3.3
H_2 0–0 S(4)	8.0251	0.85	3.35±1.10	3.41±1.13	17.1±4.6	18.1±4.8	8.16±2.69	10.5±3.5	< 106.3	< 108.3	13.3±3.3	13.8±3.4
H_2 0–0 S(5)	6.9095	0.85	10.6±2.2	10.7±2.2	40.3±6.3	41.6±6.5	14.7±4.8	16.9±5.6	< 117.4	< 118.7	24.2±4.3	24.7±4.3
H_2 0–0 S(6)	6.1086	0.85	< 6.98	< 7.06	< 25.6	< 26.5	< 16.0	< 18.9	< 214.6	< 217.2	8.41±2.78	8.62±2.84
H_2 0–0 S(7)	5.5112	0.85	< 50.2	< 50.9	35.1±7.9	36.6±8.2	9.36±3.09	11.3±3.7	< 157.5	< 159.6	24.8±6.2	25.5±6.3
H_2 0–0 S(8)	5.0531	0.85	< 9.86	< 10.0	8.14±2.69	8.53±2.81	< 2.95	< 3.64	< 64.4	< 65.4	4.61±1.25	4.75±1.29
H_2 0–0 S(9)	4.6946	0.85	< 10.9	< 11.0	30.4±10.0	32.0±10.6	< 5.75	< 7.28	< 783.4	< 797.1	< 11.7	< 12.1
H_2 0–0 S(10)	4.4099	0.85	< 25.1	< 25.6	< 6.33	< 6.70	< 4.81	< 6.23	< 32.5	< 33.1	9.79±3.23	10.2±3.35
H_2 0–0 S(11)	4.1813	0.85	< 44.4	< 45.3	6.72±2.22	7.15±2.36	< 7.75	< 10.3	< 30.7	< 31.3	< 6.41	< 6.68
[Fe I] ($^5D_4$–$^5D_3$)	24.0424	1.15	< 53.3	< 54.0	< 5.80	< 6.05	< 10.1	< 12.2	< 45.9	< 46.5	< 11.9	< 12.3
[Fe I] ($^5D_3$–$^5D_2$)	34.7135	2.01	< 5.38	< 5.42	< 14.5	< 14.8	< 59.9	< 67.3	< 33.9	< 34.2	< 47.4	< 48.1
[Fe II] ($^4F_{9/2}$–$^4F_{7/2}$)	17.9363	1.15	< 19.0	< 19.4	< 1.64	< 1.74	8.94±2.63	11.9±3.5	< 6.15	< 6.28	2.39±0.65	2.49±0.67
[Fe II] ($^6D_{9/2}$–$^6D_{7/2}$)	25.9882	1.15	< 1.84	< 1.86	3.33±1.10	3.45±1.14	52.7±11.0	62.0±12.9	< 62.1	< 62.8	6.42±2.08	6.58±2.13
[Fe II] ($^6D_{7/2}$–$^6D_{5/2}$)	35.3491	2.01	< 12.7	< 12.8	< 9.22	< 9.43	49.4±16.3	54.6±18.0	< 39.4	< 39.7	< 40.1	< 40.7
[S I] ($^3P_2$–$^3P_1$)	25.2490	1.15	< 3.35	< 3.39	5.75±1.63	5.97±1.69	< 29.6	< 35.2	< 59.8	< 60.6	7.02±2.10	7.20±2.15
[Si II] ($^2P_{1/2}$–$^2P_{3/2}$)	34.8152	2.01	23.1±7.6	23.3±7.7	30.5±10.1	31.2±10.3	1523±251	1687±279	95.2±31.4	95.9±31.7	58.6±4.1	59.4±4.2
[O I] ($^3P_2$–$^3P_1$)	63.1850	16.3	945.7±66.2	948.5±66.4	659.7±47.8	665.5±48.3	11253±1138	11717±1185	782.5±54.8	784.8±54.9	5348±298	5380±299
[O I] ($^3P_1$–$^3P_0$)	145.535	8.82	189.5±17.8	189.6±17.8	< 94.8	< 95.0	2888±290	2912±292	225.7±25.0	225.8±25.0	< 284.4	< 285.0
[C II] ($^2P_{1/2}$–$^2P_{3/2}$)	157.741	11.6	294.6±20.6	294.8±20.6	625.4±46.3	626.3±46.4	1572±159	1583±160	395.3±27.7	395.5±27.7	2245±232	2247±232
UIR (C–C stretch)	6.22	0.85	774±58	792±59	< 307	< 317	2214±166	2267±170	< 234	< 240	< 253	< 259

Table 3. (Continued)

Line	λ	Beam	Elias3–1		T Tau		HD 97048		HD 97300		HR 5999	
	[μm]	[10^{-8} sr]	Obs.	Ext. corr.	Obs.	Ext. Corr.	Obs.	Ext. Corr.	Obs.	Ext. Corr.	Obs.	Ext. Corr.
H_2 0–0 S(0)	28.2188	1.64	< 4.72	< 5.12	< 4.67	< 4.74	< 5.83	< 5.91	< 2.33	< 2.37	< 4.97	< 5.00
H_2 0–0 S(1)	17.0348	1.15	< 4.10	< 4.78	1.80$\pm$0.59	1.85$\pm$0.61	< 2.07	< 2.12	–	–	< 1.50	< 1.52
H_2 0–0 S(2)	12.2786	1.15	< 19.9	< 23.7	< 9.68	< 9.99	< 5.40	< 5.56	–	–	< 20.0	< 20.2
H_2 0–0 S(3)	9.6649	0.85	< 2.29	< 3.54	6.81$\pm$1.95	7.36$\pm$2.10	< 1.83	< 1.97	< 3.06	< 3.29	< 0.59	< 0.61
H_2 0–0 S(4)	8.0251	0.85	< 3.44	< 3.97	3.17$\pm$1.05	3.25$\pm$1.07	< 2.20	< 2.25	< 2.15	< 2.20	< 4.22	< 4.25
H_2 0–0 S(5)	6.9095	0.85	< 6.26	< 6.79	13.6$\pm$2.6	13.8$\pm$2.7	< 6.17	< 6.25	< 5.91	< 5.99	< 4.60	< 4.63
H_2 0–0 S(6)	6.1086	0.85	< 9.12	< 10.0	< 8.07	< 8.21	< 10.2	< 10.3	< 9.19	< 9.34	< 10.6	< 10.7
H_2 0–0 S(7)	5.5112	0.85	< 9.66	< 10.7	11.0$\pm$2.6	11.2$\pm$2.7	< 9.28	< 9.45	< 15.7	< 16.0	< 16.2	< 16.3
H_2 0–0 S(8)	5.0531	0.85	< 23.1	< 26.1	< 4.52	< 4.62	< 4.53	< 4.62	–	–	< 12.2	< 12.3
H_2 0–0 S(9)	4.6946	0.85	< 26.9	< 30.8	2.87$\pm$0.95	2.94$\pm$0.97	< 5.47	< 5.59	–	–	< 15.4	< 15.5
H_2 0–0 S(10)	4.4099	0.85	< 5.66	< 6.56	< 3.13	< 3.21	< 4.99	< 5.11	< 7.06	< 7.24	< 10.7	< 10.8
H_2 0–0 S(11)	4.1813	0.85	< 9.10	< 10.7	< 4.67	< 4.81	< 5.25	< 5.39	< 9.07	< 9.33	< 5.07	< 5.13
[Fe I] ($^5D_4$–$^5D_3$)	24.0424	1.15	< 2.13	< 2.37	< 1.83	< 1.87	< 3.02	< 3.07	< 1.52	< 1.54	< 0.89	< 0.90
[Fe I] ($^5D_3$–$^5D_2$)	34.7135	2.01	< 4.70	< 4.98	< 1.04	< 1.05	< 3.45	< 3.48	< 2.32	< 2.35	< 5.85	< 5.87
[Fe II] ($^4F_{9/2}$–$^4F_{7/2}$)	17.9363	1.15	< 6.74	< 7.94	0.52$\pm$0.17	0.53$\pm$0.18	< 1.85	< 1.90	–	–	< 1.43	< 1.44
[Fe II] ($^6D_{9/2}$–$^6D_{7/2}$)	25.9882	1.15	< 2.29	< 2.51	1.85$\pm$0.61	1.88$\pm$0.62	< 2.86	< 2.90	< 1.41	< 1.43	< 1.26	< 1.27
[Fe II] ($^6D_{7/2}$–$^6D_{5/2}$)	35.3491	2.01	< 3.86	< 4.08	4.23$\pm$1.40	4.28$\pm$1.41	< 4.98	< 5.03	–	–	< 6.98	< 7.00
[S I] ($^3P_2$–$^3P_1$)	25.2490	1.15	< 2.59	< 2.86	4.09$\pm$1.28	4.16$\pm$1.30	< 1.80	< 1.83	< 0.70	< 0.71	< 1.24	< 1.25
[Si II] ($^2P_{1/2}$–$^2P_{3/2}$)	34.8152	2.01	< 6.32	< 6.70	12.6$\pm$4.2	12.7$\pm$4.2	< 3.80	< 3.84	< 2.24	< 2.26	< 2.63	< 2.64
[O I] ($^3P_2$–$^3P_1$)	63.1850	16.3	–	–	234.8$\pm$23.5	235.8$\pm$23.6	19.0$\pm$3.0	19.1$\pm$3.0	–	–	–	–
[O I] ($^3P_1$–$^3P_0$)	145.535	8.82	–	–	< 14.9	< 14.9	–	–	–	–	–	–
[C II] ($^2P_{1/2}$–$^2P_{3/2}$)	157.741	11.6	–	–	10.3$\pm$1.9	10.3$\pm$1.9	7.01$\pm$1.04	7.02$\pm$1.04	–	–	–	–
UIR (C–C stretch)	6.22	0.85	413$\pm$31	453$\pm$34	< 161	< 164	440$\pm$33	446$\pm$34	–	–	< 293	< 294

Line	λ	Beam	R CrA		T CrA		WW Vul		BD+40°4124		LkHα 224		HD 200775	
	[μm]	[10^{-8} sr]	Obs.	Ext. corr.	Obs.	Ext. Corr.	Obs.	Ext. Corr.	Obs.	Ext. Corr.	Obs.	Ext. Corr.	Obs.	Ext. Corr.
H_2 0–0 S(0)	28.2188	1.64	< 11.4	< 11.7	< 6.04	< 6.14	< 1.78	< 1.80	< 6.60	< 6.81	< 9.51	< 9.81	< 6.04	< 6.17
H_2 0–0 S(1)	17.0348	1.15	< 10.7	< 11.2	3.96$\pm$1.31	4.09$\pm$1.35	< 0.75	< 0.77	5.37$\pm$1.77	5.69$\pm$1.88	10.1$\pm$3.3	10.7$\pm$3.5	< 3.24	< 3.37
H_2 0–0 S(2)	12.2786	1.15	< 46.0	< 48.3	5.58$\pm$1.68	5.80$\pm$1.74	< 9.84	< 10.1	7.12$\pm$2.35	7.62$\pm$2.51	12.7$\pm$4.2	13.6$\pm$4.5	< 5.32	< 5.56
H_2 0–0 S(3)	9.6649	0.85	< 6.40	< 7.25	< 2.09	< 2.29	< 0.95	< 1.01	7.74$\pm$2.36	9.15$\pm$2.79	9.81$\pm$3.12	11.6$\pm$3.7	< 2.13	< 2.37
H_2 0–0 S(4)	8.0251	0.85	< 20.3	< 21.2	< 3.14	< 3.23	< 4.34	< 4.42	1.02$\pm$0.34	1.08$\pm$0.36	6.89$\pm$2.27	7.28$\pm$2.40	< 2.75	< 2.85
H_2 0–0 S(5)	6.9095	0.85	< 28.9	< 29.6	< 4.04	< 4.11	< 1.65	< 1.67	2.45$\pm$0.81	2.53$\pm$0.83	11.7$\pm$2.5	12.1$\pm$2.6	< 5.22	< 5.33
H_2 0–0 S(6)	6.1086	0.85	< 19.5	< 20.0	< 20.1	< 20.5	< 5.05	< 5.11	< 7.96	< 8.25	< 6.26	< 6.49	< 7.65	< 7.83
H_2 0–0 S(7)	5.5112	0.85	< 25.9	< 26.7	< 10.7	< 10.9	< 14.7	< 14.9	< 8.10	< 8.44	< 13.0	< 13.5	< 12.2	< 12.6
H_2 0–0 S(8)	5.0531	0.85	< 12.3	< 12.7	< 6.76	< 6.93	< 15.7	< 16.0	< 18.3	< 19.2	< 35.5	< 37.2	< 7.06	< 7.27
H_2 0–0 S(9)	4.6946	0.85	< 17.6	< 18.3	< 4.86	< 5.00	< 15.5	< 15.8	< 11.6	< 12.2	< 25.5	< 26.9	< 17.3	< 17.9
H_2 0–0 S(10)	4.4099	0.85	< 35.2	< 36.8	< 6.10	< 6.29	< 7.37	< 7.50	< 4.17	< 4.41	< 4.15	< 4.40	< 10.3	< 10.7
H_2 0–0 S(11)	4.1813	0.85	< 30.0	< 31.5	< 6.70	< 6.93	< 10.5	< 10.7	< 7.37	< 7.85	< 10.8	< 11.5	< 18.4	< 19.2
[Fe I] ($^5D_4$–$^5D_3$)	24.0424	1.15	< 5.02	< 5.18	< 0.68	< 0.69	< 1.26	< 1.28	< 1.72	< 1.79	< 1.46	< 1.53	< 2.05	< 2.10
[Fe I] ($^5D_3$–$^5D_2$)	34.7135	2.01	< 8.35	< 8.49	< 4.14	< 4.19	< 3.90	< 3.93	< 4.00	< 4.09	< 4.86	< 4.97	< 3.89	< 3.94
[Fe II] ($^4F_{9/2}$–$^4F_{7/2}$)	17.9363	1.15	< 3.96	< 4.15	< 0.89	< 0.92	< 0.85	< 0.86	< 0.97	< 1.03	< 1.86	< 1.98	< 1.10	< 1.15
[Fe II] ($^6D_{9/2}$–$^6D_{7/2}$)	25.9882	1.15	1.33$\pm$0.44	1.36$\pm$0.45	< 1.14	< 1.17	< 1.10	< 1.12	0.69$\pm$0.23	0.71$\pm$0.23	< 2.23	< 2.31	< 1.89	< 1.93
[Fe II] ($^6D_{7/2}$–$^6D_{5/2}$)	35.3491	2.01	< 4.76	< 4.84	< 4.07	< 4.12	< 4.19	< 4.22	< 4.40	< 4.50	< 7.70	< 7.86	< 3.81	< 3.87
[S I] ($^3P_2$–$^3P_1$)	25.2490	1.15	6.78$\pm$2.05	6.97$\pm$2.10	< 0.82	< 0.84	< 0.65	< 0.65	< 1.37	< 1.42	1.60$\pm$0.52	1.66$\pm$0.54	< 1.26	< 1.29
[Si II] ($^2P_{1/2}$–$^2P_{3/2}$)	34.8152	2.01	9.38$\pm$3.09	9.54$\pm$3.15	< 3.63	< 3.67	< 2.92	< 2.94	23.2$\pm$7.7	23.7$\pm$7.8	24.2$\pm$8.0	24.8$\pm$8.2	19.0$\pm$6.3	19.3$\pm$6.4
[O I] ($^3P_2$–$^3P_1$)	63.1850	16.3	681.4$\pm$47.6	684.9$\pm$47.9	–	–	–	–	703.6$\pm$49.5	709.9$\pm$49.9	–	–	714.4$\pm$72.8	718.5$\pm$73.2
[O I] ($^3P_1$–$^3P_0$)	145.535	8.82	< 40.0	< 40.1	–	–	–	–	41.5$\pm$4.0	41.6$\pm$4.0	–	–	297.4$\pm$29.8	297.7$\pm$29.8
[C II] ($^2P_{1/2}$–$^2P_{3/2}$)	157.741	11.6	35.7$\pm$5.5	35.8$\pm$5.5	–	–	–	–	517.5$\pm$36.4	518.3$\pm$36.4	–	–	329.6$\pm$33.1	330.0$\pm$33.1
UIR (C–C stretch)	6.22	0.85	< 270	< 277	< 106	< 108	< 192	< 194	260$\pm$20	269$\pm$20	< 135	< 140	< 132	< 135

Table 4. Observed (Obs.) and extinction corrected (EC) data for shocks and PDRs from literature. Numbers in brackets indicate the errors in the last digits.

Line	Orion BN/KL				IC 443				RCW 103			
	Obs.	EC	Beam	Ref.	Obs.	EC	Beam	Ref.	Obs.	EC	Beam	Ref.
	[10^{-3} erg s^{-1}	cm^{-2} sr^{-1}]	[10^{-8} sr]		[10^{-3} erg s^{-1}	cm^{-2} sr^{-1}]	[10^{-8} sr]		[10^{-3} erg s^{-1}	cm^{-2} sr^{-1}]	[10^{-8} sr]	
H_2 0–0 S(1) 17.03 μm	3.3(6)	4.0(7)	0.01	(1)	–	–	–	–	0.11(3)	0.12(3)	1.15	(13)
H_2 1–0 S(1) 2.122 μm	8.4(8)	18.0(17)	0.06	(2)	0.637(2)	1.172(3)	0.05	(7)	0.386(12)	0.544(17)	0.11	(14)
H_2 2–1 S(1) 2.248 μm	0.85(10)	1.67(20)	0.06	(2)	0.0547(5)	0.0937(9)	0.05	(7)	0.047(10)	0.064(14)	0.11	(14)
[S I] 25.25 μm	3.9(6)	4.4(7)	2.45	(3)	–	–	–	–	< 0.01	< 0.01	1.15	(13)
[Si II] 34.82 μm	6.1(6)	6.6(6)	3.27	(3)	0.26(3)	0.27(4)	2.01	(8)	1.4(2)	1.4(2)	2.01	(13)
[O I] 63.18 μm	56(20)	58(21)	2.15	(4)	2.26(19)	2.31(19)	2.51	(9)	0.44(5)	0.44(5)	15.3	(13)
[O I] 145.5 μm	–	–	–	–	–	–	–	–	0.037(8)	0.037(8)	15.3	(13)
[C II] 157.7 μm	3.9(5)	3.9(5)	7.24	(5)	0.39(8)	0.39(8)	2.61	(10)	0.54(6)	0.54(6)	15.3	(13)
A_V [^{m}]		10.0		(1)		8.0		(11)		4.5		(14)
d [pc]		430		(6)		1500		(12)		6600		(15)

Line	Orion Bar				NGC 2023				S140			
	Obs.	EC	Beam	Ref.	Obs.	EC	Beam	Ref.	Obs.	EC	Beam	Ref.
	[10^{-3} erg s^{-1}	cm^{-2} sr^{-1}]	[10^{-8} sr]		[10^{-3} erg s^{-1}	cm^{-2} sr^{-1}]	[10^{-8} sr]		[10^{-3} erg s^{-1}	cm^{-2} sr^{-1}]	[10^{-8} sr]	
H_2 0–0 S(1) 17.03 μm	0.110(5)	0.121(6)	0.06	(16)	0.022(4)	0.022(4)	1.15	(21)	0.020(6)	0.022(6)	1.15	(25)
H_2 1–0 S(1) 2.122 μm	0.078(13)	0.114(19)	0.15	(17)	0.060(2)	0.067(2)	0.92	(22)	0.16(2)	0.22(3)	0.03	(26)
H_2 2–1 S(1) 2.248 μm	0.008(4)	0.011(6)	0.15	(18)	0.016(2)	0.018(2)	0.92	(22)	–	–	–	–
[S I] 25.25 μm	< 0.13	< 0.14	2.45	(10)	–	–	–	–	–	–	–	
[Si II] 34.82 μm	9.0(5)	9.3(5)	5.51	(19)	0.20(11)	0.20(11)	3.10	(23)	0.030(9)	0.032(9)	2.01	(25)
[O I] 63.18 μm	54(5)	55(5)	2.15	(5)	3.62(10)	3.63(10)	2.61	(23)	0.33(10)	0.33(10)	15.3	(27)
[O I] 145.5 μm	4.2(5)	4.2(5)	6.72	(5)	0.23(4)	0.23(4)	4.42	(23)	–	–	–	–
[C II] 157.7 μm	3.4(5)	3.4(5)	7.24	(5)	0.68(4)	0.68(4)	4.22	(23)	0.35(11)	0.35(11)	15.3	(27)
A_V [^{m}]		5.0		(20)		1.4		(24)		4.0		(25)
d [pc]		430		(6)		475		(24)		910		(28)

References to Table 4: (1) Parmar et al. (1994); (2) Brand et al. (1988); (3) Haas et al. (1991); (4) Crawford et al. (1986); (5) Stacey et al. (1993); (6) Warren & Hesser (1978); (7) Richter et al. (1995a); (8) Oliva et al. (1999a); (9) Burton et al. (1990b); (10) Haas (1997); (11) van Dishoeck et al. (1993); (12) Burton et al. (1988); (13) Oliva et al. (1999b); (14) Oliva et al. (1990); (15) Leibowitz & Danziger (1983); (16) Parmar et al. (1991); (17) Burton et al. (1990a); (18) Hayashi et al. (1985); (19) Haas et al. (1986); (20) Assumed; (21) This paper; (22) Hasegawa et al. (1987); (23) Steiman-Cameron et al. (1997); (24) Jaffe et al. (1990); (25) Timmermann et al. (1996). (26) Carr (1990); (27) Emery et al. (1996); (28) Crampton & Fisher (1974).

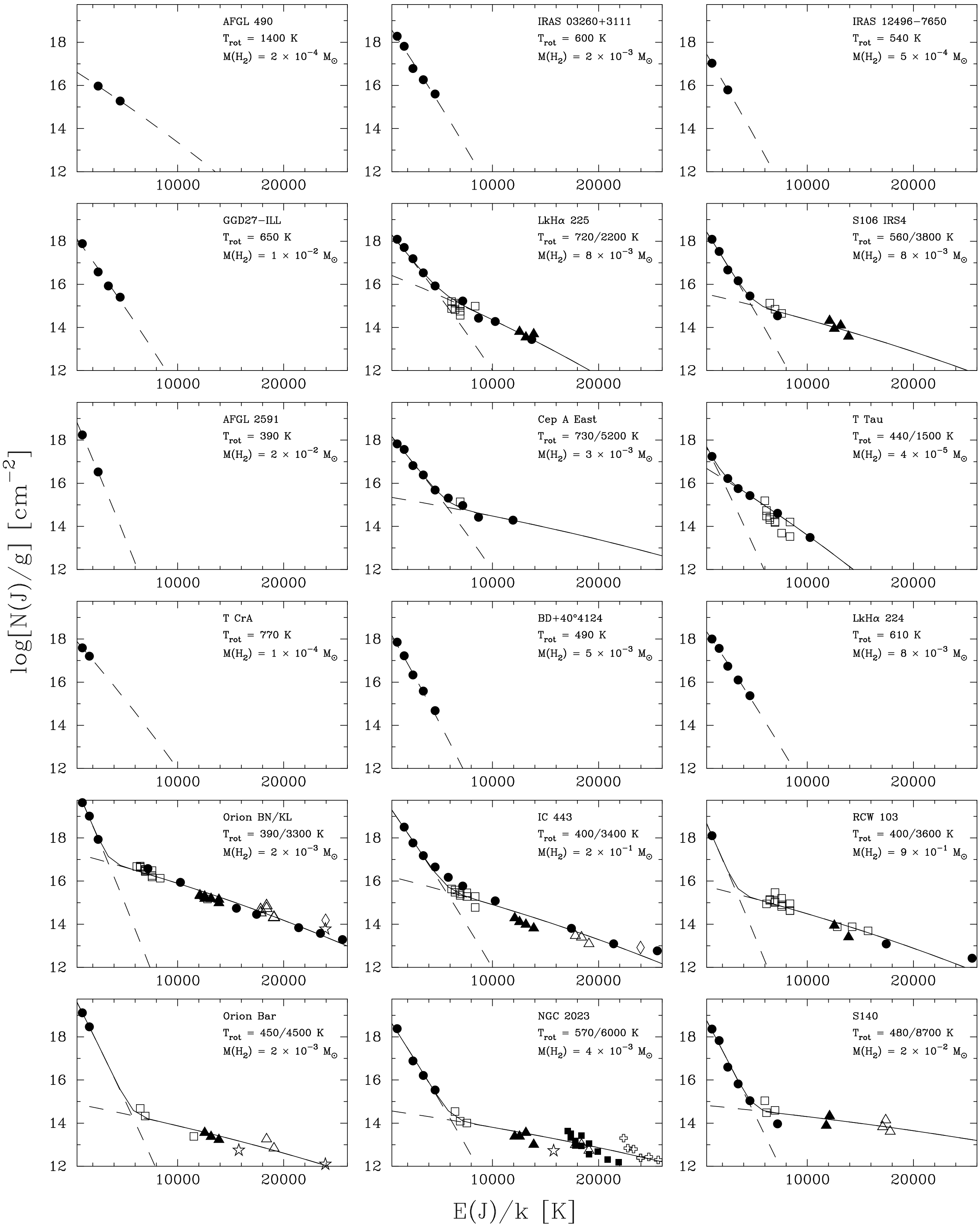

Fig. 2. H_2 excitation diagrams for programme and comparison stars. Shown are apparent columns of H_2 in the pure-rotational (0–0) transitions (filled dots), 1–0 transitions (open squares), 2–1 transitions (filled triangles), 2–0 transitions (open stars), 3–2 transitions (open triangles), 3–0 transitions (filled squares), 4–3 transitions (open diamonds), and 4–1 transitions (open crosses). Observational errors are smaller than the size of the plot symbol. The Boltzmann distribution fits are plotted as dashed lines. The solid lines show the sum of both thermal components for each source.

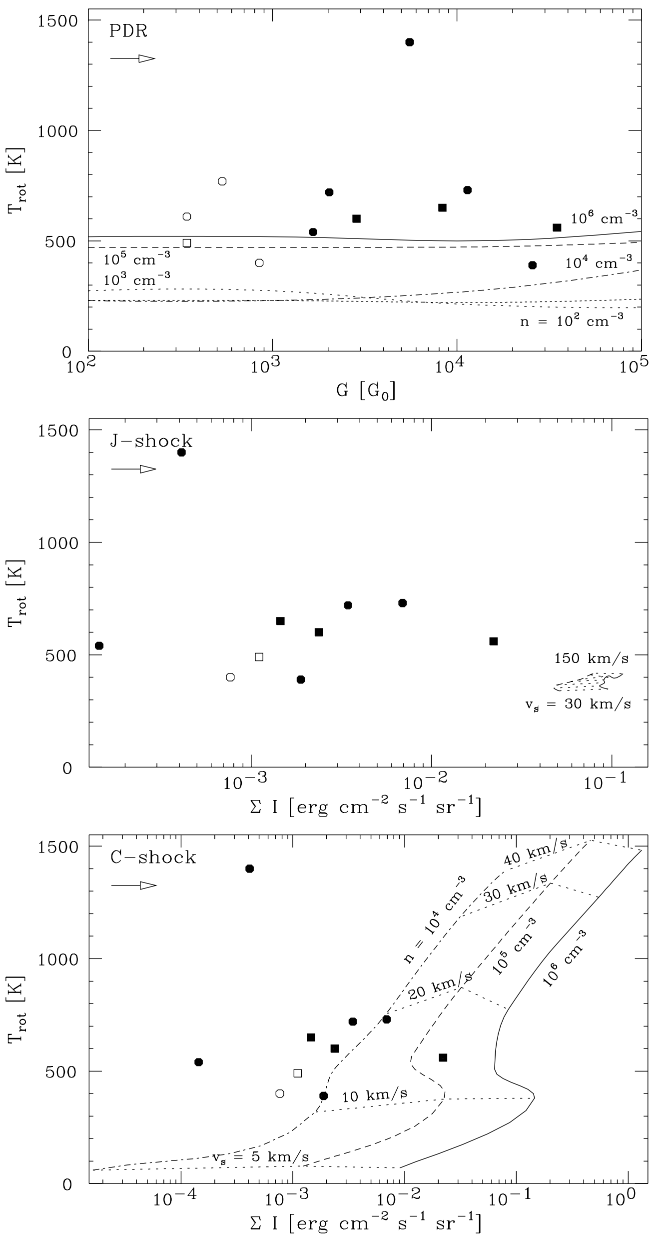

Fig. 3. Comparison of observed H_2 rotational temperatures to theoretical relation between continuum fluxes and $T_{\rm rot}$ (PDR models) or summed intensity in all observed lines and $T_{\rm rot}$ (shocks). Sources which show PAH emission are plotted as squares. Plot symbols are filled for Class I sources. The arrows show the direction of beam dilution.

assuming a beam filling factor of one. The resulting G-values, listed in Table 6, were used to plot our observations directly in the parameter space of the PDR models (Fig. 3). Note that if the extent of the PDR is smaller than the beam size, as might be expected for some sources, our data points in Fig. 4 may be shifted along the direction indicated by the arrows. However, for PDRs the resulting $T_{\rm rot}$ does not depend much on G, so this does not introduce an additional uncertainty in our analysis.

Table 5. Results of H_2 Boltzmann distribution fits.

Object	$T_{\rm rot}$ [K]	$N_{\rm rot}$ [cm^{-2}]	$T_{\rm vib}$ [K]	$N_{\rm vib}$ [cm^{-2}]	$M(H_2)$ [M$_\odot$]
AFGL 490	1400	1.9×10^{18}	–	–	2×10^{-4}
IRAS03260+3111	600	1.2×10^{20}	–	–	2×10^{-3}
IRAS12496−7650	540	9.1×10^{18}	–	–	5×10^{-4}
GGD 27-ILL	650	4.2×10^{19}	–	–	1×10^{-2}
LkHα 225	720	6.7×10^{19}	2200	1.7×10^{18}	8×10^{-3}
S106 IRS4	560	8.7×10^{19}	3800	3.6×10^{17}	8×10^{-3}
AFGL 2591	390	2.2×10^{20}	–	–	2×10^{-2}
Cep A East	730	5.0×10^{19}	5200	3.0×10^{17}	3×10^{-3}
T Tau	440	1.5×10^{19}	1500	2.1×10^{18}	4×10^{-5}
T CrA	770	2.7×10^{19}	–	–	1×10^{-4}
BD+40°4124	490	4.8×10^{19}	–	–	5×10^{-3}
LkHα 224	610	7.0×10^{19}	–	–	8×10^{-3}
Orion BN/KL	390	6.1×10^{21}	3300	1.7×10^{19}	2×10^{-3}
IC 443	610	6.5×10^{20}	3400	1.5×10^{18}	2×10^{-1}
RCW 103	400†	1.6×10^{20}	3600	5.5×10^{17}	9×10^{-1}
Orion Bar	450	1.3×10^{21}	4500	9.1×10^{16}	2×10^{-3}
NGC 2023	570	1.4×10^{20}	6000	5.7×10^{16}	4×10^{-3}
S140	480	1.9×10^{20}	8700	1.4×10^{17}	2×10^{-2}

† Assumed temperature.

For the shocks, a direct comparison between theory and observation is more cumbersome. We have decided to plot the results of the $T_{\rm rot}$ fits from the J- and C-shock models versus the total flux observed in all lines (Fig. 3). Since [O I] 63.2 μm, [C II] 157.7 μm and [Si II] 34.8 μm are expected to be the dominant coolants in the lines we study here, we only plot this quantity in sources where these three lines were measured. It is also given in Table 6. For shocks with velocities in excess of 20 km s^{-1}, Lyα is also an important coolant, which we have neglected here. The total luminosity of the cooling in a shock is proportional to nv_s^3, so for the shocks plotted in Fig. 3 the ordinate will no longer directly correspond to a single parameter in the models, and instead of the simple lines for the PDRs, we get a grid of models with different shock parameters. We are also left with the additional uncertainty that the shock will likely not fill the entire beam, so our data points must be shifted along a vector indicated in the figures to take this into account.

Comparing the excitation temperature of the template sources listed in Table 5 with the ones plotted in Fig. 2, we note that for the relatively clean PDRs S140 and the Orion Bar, the derived excitation temperature falls within the range predicted by PDR models. Although the Tielens & Hollenbach (1985) models do not predict a detailed ro-vibrational H_2 spectrum, competing PDR models (e.g. Black & van Dishoeck 1987; Draine & Bertoldi 1996) also show the same hot component which we observe in these PDR template sources. This hot PDR may reflect the combined effects of UV-pumped infrared fluorescence and the presence of a very warm, but thin, surface layer.

The only shock template source for which we were able to derive a reliable $T_{\rm rot}$, Orion BN/KL peak 1, agrees well with the value expected for a J-shock. Note however that all three of our template shock sources also show evidence for a hot H_2 component, which is not predicted by J-shock models. This probably means that even in these relatively clean template cases, we do not observe a single J-shock, but a combination of one or more J- and C-shocks. Possibly this reflects the presence of shocked clumps of gas where the J-shock corresponds to the region around the point of impact while the C-shock emission originates from oblique shocks further away.

The situation for the programme sources is distinctly less clear-cut. Except for GGD 27-ILL and IRAS 03260+3111, which appear somewhat warmer in pure rotational H_2 than predicted by the models, all sources which show PAH emission and might therefore be expected to be dominated by PDR emission have excitation temperatures within the range predicted by the PDR models. Small differences between observations and the models may reflect the fact that these observations spatially resolve the PDR while the models refer to integrated (i.e. averaged) values. Of the remaining sources, only AFGL 2591 has an excitation temperature compatible with the J-shock models. All are compatible with excitation temperatures expected for C-shocks. However, in the next section we will show that the observed atomic fine-structure spectrum in these sources does require the presence of a J-shock. This could either mean that the H_2 has a stronger C-shock component than the template sources, or that the J-shock models of Hollenbach & McKee (1989) underestimate the temperature in the post-shock gas, where the H_2 emission originates in a J-shock. We will come back to this in the discussion and argue that the latter explanation is more likely.

5. Fine structure lines

In order to interpret our observations as arising in either a PDR, a C-Shock or a J-shock, we compare our results with the line fluxes predicted by theoretical models of such regions (Tielens & Hollenbach 1985; Hollenbach & McKee 1989; Kaufman & Neufeld 1996). Since the *Infrared Space Observatory* offers the first possibility to confront the infrared spectrum predicted by these models with a wide range of astronomical objects, and the physics behind these models is still not completely understood, there are significant uncertainties in such a procedure. Therefore we also again compare our results with observations from literature of the template sources containing shocks and PDRs.

In Figs. 4–6 we have plotted the absolute line intensities predicted either against the G-values computed from the infrared luminosity (PDRs) or against the sum of all observed lines fluxes (shocks), computed in the previous section. Note that since the quantities plotted on both axes of these plots depend on the beam filling factor, the points may be expected to shift along the arrows shown in the plots in case the PDR or shock is smaller than the beam size.

By comparing the predicted line fluxes for the PDR, J-shock and C-shock models with our observations in Figs. 4–6 we can directly draw several interesting conclusions. The predicted intensity in the [Fe I] and [S I] lines is orders of magnitudes higher in the shock models than in the PDR models, because in the latter nearly all iron and sulfur will be ionized in the heated surface layer of a PDR. [Fe I] was not detected in any source within our sample. However, [S I] 25.3 μm emission was detected for seven sources. Comparing the location of these line fluxes in Fig. 4 with the PDR model prediction we see that the observed [S I] fluxes are too high to be compatible with a PDR origin, even for PDRs as dense as 10^6 cm^{-3}. This means that *the detection of [S I] emission with ISO can only mean that a shock is present*. Also note that the detection of [S I] and PAHs appear mutually exclusive in our sample (Table 6), suggesting that these may be a fast and relatively straightforward way to distinguish PDRs and shocks.

By definition, C-shocks cannot produce ionized species like [Fe II], [Si II] and [C II]. The last species may still be detected in such regions because it will also reach observable strengths in PDRs illuminated by weak FUV fields (c.f. Fig. 4), such as the diffuse galactic background emission ($G \approx 1$). Since the [C II] line fluxes listed in Table 3 are not corrected for background emission, we cannot draw conclusions from just the detection of [C II]. However, the mere detection of [Si II] or [Fe II] means that either a PDR or a J-shock must be present within the ISO-SWS beam. For most sources in which we have detected [Si II] or [Fe II] emission, it can be well explained by either the PDR or the J-shock models (Figs. 4–5). In only one case, S106 IRS4, is the observed [Si II] 34.8 μ line intensity clearly too strong to be explained by either PDR or J-shock models. However, van den Ancker et al. (2000b) found that the infrared spectrum of this source is dominated by its associated H II region, which will also contribute to the [Si II] and [Fe II] lines studied here.

Although both the PDR and the J-shock models predict the presence of observable amounts of [C II] emission, the expected line strength in PDRs of moderate to high density ($\geq 10^3$ cm^{-3}) is more than an order of magnitude higher than in J-shocks. Most of the sources with observed [C II] 158 μm emission have strengths that are too high to be explained by the J-shock models. For these sources we can therefore immediately infer that they must be due to a PDR. For the remainder of the sources, the [C II] 158 μm line strength becomes comparable to the one expected for the background, so a direct comparison of those values to J-shock models will yield inconclusive results.

Intense [O I] 63.2 μm emission can be produced by PDRs, as well as J- and C-shocks. The observed [O I] 63.2 μm intensities are all within the range that can be reproduced by the models. The [O I] 145.5 μm line can also be produced by the PDR and C-shock models; the J-shock models predict less [O I] 146 μm emission than is observed. Also, in nearly all the cases we study here, the PDR or C-shock model parameters found from the [O I] 63.2 and 145.5 μm lines do not agree with each other; either the [O I] 63.2 μm line appears too weak, or the [O I] 145.5 μm line appears too strong. Such a discrepancy is not unique to the sources we study here. It has also been observed in spatially resolved PDRs (Liseau et al. 1999), so it cannot be caused by the different LWS beam sizes at 63 and 146 microns. One pos-

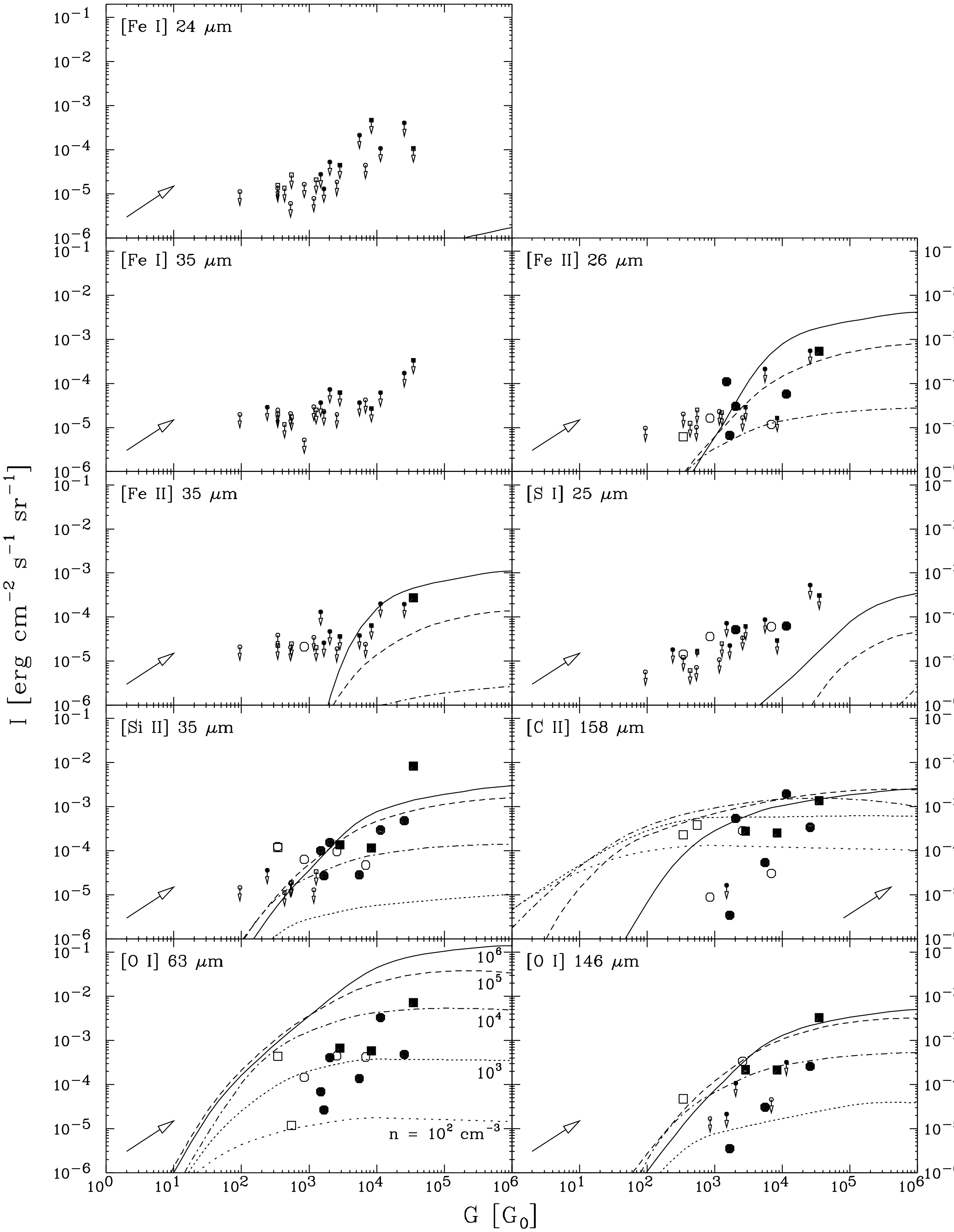

Fig. 4. Comparison of observed fine-structure line intensities and continuum flux to the PDR models. Sources which show PAH emission are plotted as squares. The large arrows show the direction of beam dilution.

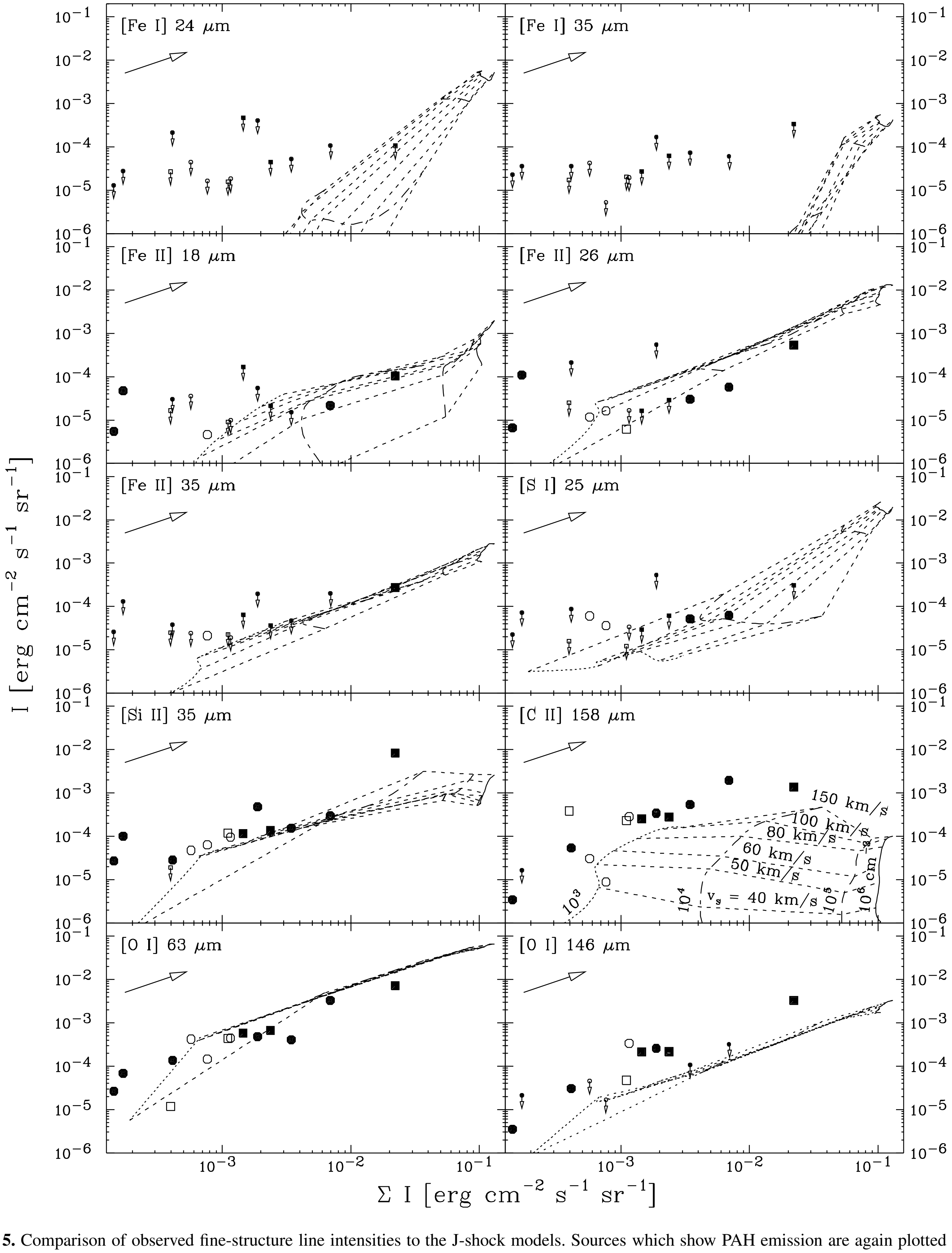

Fig. 5. Comparison of observed fine-structure line intensities to the J-shock models. Sources which show PAH emission are again plotted as squares. The large arrows show the direction of beam dilution.

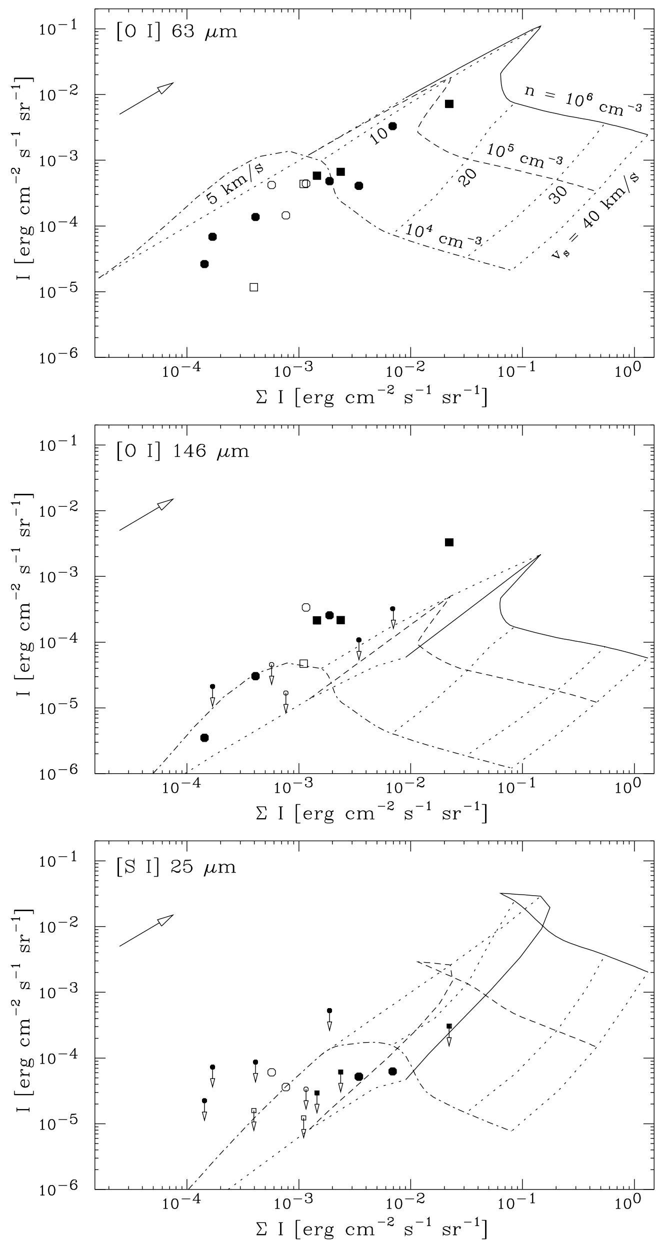

Fig. 6. Comparison of observed fine-structure line intensities to the C-shock models. Sources with PAH emission are plotted as squares. The large arrows show the direction of beam dilution.

sible explanation would be that [O I] 145.5 μm is blended with the CO J=18–17 line. In view of the strength of other CO lines in our LWS spectra, this line is in general expected to be too weak to dominate the line flux, and thus cannot account for the observed anomaly. Another, more promising, explanation may be that the [O I] 63.2 μm line intensity has been diminished by absorption by cool foreground material. [O I] 63.2 μm absorption has indeed been found in the line of sight towards a few sources (Poglitsch et al. 1996; Kraemer et al. 1998), lending credence to the suggestion that this may also be the case in our sources. Note that if this suggestion is correct, this means that the observed [O I] emission in *all* our sources must come from either PDRs or C-shocks, since the [O I] 145.5 μm line fluxes are too high compared to the J-shock models.

Physical parameters for each star's circumstellar environment, estimated from the different measured species, as well as the likely underlying physical mechanism, are listed in Table 6.

6. Notes on individual objects

AFGL 490 (IRAS 03236+5836) is a luminous infrared source, powering a strong bipolar CO outflow with an extent of $\approx 100''$ (Lada & Harvey 1981). The central peak in AFGL 490 is believed to be an embedded intermediate-mass YSO and the driving source for the molecular outflow (Minchin et al. 1991; Haas et al. 1992). Ground-based H_2 1–0 S(1) images (Davis et al. 1998) show several knots of shocked molecular gas in the AFGL 490 outflow as well as diffuse H_2 emission, suggesting a composite origin for the emission lines detected with ISO. The temperatures derived from the H_2 0–0 S(3) and S(5) lines can only be explained by a non-dissociative shock. However, the detection of strong [Si II] and [O I] emission show that either a PDR or a fast J-shock must be present as well.

IRAS 03260+3111 was found to be a candidate for a class of objects making the transition between Class I and II YSOs by Magnier et al. (1999). Strong PAH-emission in the SWS spectrum suggests that it has a significant PDR contribution. The lines detected confirm this hypothesis: The [Si II], [O I] and [C II] are strongly suggestive of a PDR origin. The temperature of the H_2 is somewhat higher than that expected for a PDR, but this may be influenced by an apparent discontinuity between the 0–0 S(2) and S(3) lines, where SWS uses apertures of different sizes.

L1489 IRS (IRAS 04016+2610) is a Class I source in an extended molecular gas core in the Taurus star forming region. It powers a low-velocity molecular outflow adjacent to the source (Myers et al. 1988; Hogerheijde et al. 1998) and has been suggested as the powering source of a more extended molecular outflow (Terebey et al. 1989; Moriarty-Schieven et al. 1992). Recent HST NICMOS images of the source reveal a bright near-infrared nebula crossed by a dark lane, interpreted as an optically thick disk seen in silhouette (Padgett et al. 1999). Ground-based images in the H_2 1–0 S(1) line reveal strong H_2 emission from the HH 360a knot in the molecular outflow (Gómez et al. 1997). No emission lines were detected with ISO, suggesting that the shocked material in the region is confined to these small knots.

L1551 IRS5 (IRAS 04287+1801) is one of the best studied embedded YSOs. The bipolar molecular outflow emanating from L1551 IRS5 was the first to be discovered (Snell et al. 1980), and it remains a text-book example of a Class I source. It illuminates the reflection nebula HH 102, and drives both a strong molecular outflow as well as a highly collimated jet, as traced by a number of Herbig-Haro objects with high proper motions (Mundt et al. 1991; Staude & Elsässer 1993). Interferometry of L1551 IRS5 at mm wavelengths (Keene & Masson 1990) reveals the source to consist of two distinct components: an envelope with radius $\approx 12''$ and a compact structure of $\approx$

Table 6. Results of line analysis.

Object	F_{IR} [W m^{-2}]	$G_{\rm av.}$ [G$_0$]	PAH	ΣI [erg cm^{-2} s^{-1} sr^{-1}]	n [cm^{-3}] H$_2$	[Fe I]	[Fe II]	[S I]	[Si II]	[O I]	[C II]	Type
AFGL 490	1.4×10^{-10}	5.5×10^{3}	–	4.1×10^{-4}	–	–	–	–	$\gtrsim 10^{3}$	$\gtrsim 10^{3}$	–	Shock?
IRAS03260+3111	7.4×10^{-11}	2.9×10^{3}	$\surd$	2.4×10^{-3}	$\gtrsim 10^{6}$	–	–	–	$\gtrsim 10^{5}$	$> 10^{3}$	$> 10^{2}$	PDR
L1489 IRS	6.2×10^{-12}	2.4×10^{2}	–	–	–	–	–	–	–			–
L1551 IRS5	3.9×10^{-11}	1.5×10^{3}	–	1.7×10^{-4}	–	–	$\gtrsim 10^{4}$	–	$\geq 10^{3}$	$\gtrsim 10^{3}$	–	Shock?
IRAS12496−7650	4.3×10^{-11}	1.7×10^{3}	–	1.4×10^{-4}	–	–	$\geq 10^{2}$	–	$\geq 10^{3}$	$\gtrsim 10^{3}$	–	Shock?
GGD 27-ILL	2.2×10^{-10}	8.3×10^{3}	$\surd$	1.5×10^{-3}	$\gtrsim 10^{6}$	–	–	–	$\geq 10^{4}$	$\gtrsim 10^{3}$	$> 10^{2}$	PDR
LkHα 225	5.3×10^{-11}	2.0×10^{3}	–	3.4×10^{-3}	$\geq 10^{4}$	–	$\gtrsim 10^{4}$	$\geq 10^{4}$	$\geq 10^{4}$	$\gtrsim 10^{4}$	–	Shock
S106 IRS4	9.1×10^{-10}	3.5×10^{4}	$\surd$	2.2×10^{-2}	$\approx 10^{6}$	–	$> 10^{5}$	–	–	$\geq 10^{4}$	$> 10^{3}$	PDR
AFGL 2591	6.7×10^{-10}	2.6×10^{4}	–	1.9×10^{-3}	$\geq 10^{4}$	–	–	–	$> 10^{3}$	$\geq 10^{3}$	$\gtrsim 10^{3}$	PDR?
Cep A East	3.0×10^{-10}	1.1×10^{4}	–	6.9×10^{-3}	$\gtrsim 10^{4}$	–	$\geq 10^{4}$	$\gtrsim 10^{4}$	$\geq 10^{4}$	$\gtrsim 10^{4}$	–	Shock
Elias 3-1	3.3×10^{-11}	1.3×10^{3}	$\surd$	–	–	–	–	–	–			–
T Tau	2.2×10^{-11}	8.5×10^{2}	–	7.7×10^{-4}	$\gtrsim 10^{4}$	–	$\geq 10^{3}$	$\geq 10^{3}$	$\geq 10^{3}$	$\geq 10^{3}$	–	Shock†
HD 97048	1.4×10^{-11}	5.5×10^{2}	$\surd$	4.0×10^{-4}	–	–	–	–	–	$\geq 10^{2}$	–	PDR
HD 97300	1.1×10^{-11}	4.3×10^{2}	$\surd$	–	–	–	–	–	–			–
HR 5999	3.0×10^{-11}	1.2×10^{3}	–	–	–	–	–	–	–			–
R CrA	1.8×10^{-10}	6.9×10^{3}	–	5.7×10^{-4}	–	–	$\gtrsim 10^{3}$	$\geq 10^{3}$	$\geq 10^{3}$	$\gtrsim 10^{3}$	–	Shock†
T CrA	1.4×10^{-11}	5.3×10^{2}	–	–	–	–	–	–	–			–
WW Vul	2.5×10^{-12}	9.4×10^{1}	–	–	–	–	–	–	–			–
BD+40°4124	9.0×10^{-12}	3.4×10^{2}	$\surd$	1.1×10^{-3}	$\gtrsim 10^{4}$	–	$\geq 10^{5}$	–	–	$\gtrsim 10^{4}$	$\geq 10^{3}$	PDR
LkHα 224	8.9×10^{-12}	3.4×10^{2}	–	–	–	–	–	–	–			Shock†
HD 200775	6.7×10^{-11}	2.6×10^{3}	–	1.2×10^{-3}	–	–	–	–	$\gtrsim 10^{4}$	$\gtrsim 10^{3}$	$\gtrsim 10^{3}$	PDR

† Probably not connected to optical source.

0.″3, presumably an accretion disk of a similar size as the solar system. Diffuse H_2 1–0 S(1) emission in the L1551 region was observed by Yamashita & Tamura (1992), and later shown to have a patchy structure by Davis et al. (1995), which may be due to gas which is shock-heated by the strong wind from IRS5. No compact H_2 knots similar to those observed in the surroundings of other YSOs were found in the large-scale surroundings of L1551 IRS5 (Gómez et al. 1997), suggesting the presence of shocks sufficiently powerful to destroy the dust required to re-form molecular hydrogen in post-shock gas. [Fe II], [Si II] and [O I] emission was detected by ISO. In view of the previous discussion it seems likely that this will be shock excited.

IRAS 12496−7650 (DK Cha) is an embedded active young stellar object located in the Chamaeleon II dark cloud. It is associated with a weak molecular outflow (Knee 1992) and possibly drives a collimated jet (Hughes et al. 1991). It is associated with the Herbig-Haro objects HH 52–54, some of which are also included in the ISO beam. If the H_2 ortho-/para-ratio in these objects is smaller than the high-temperature equilibrium value of 3, as suggested by ISO spectroscopy of HH 54 (Neufeld et al. 1998), our estimate of the H_2 mass (Table 5) will be too low. The ISO [O I]/[C II] ratio suggests a strong shock component to be present in the infrared emission-line spectrum. In view of the detected [Fe II] and [Si II] emission, this shock must be of J-type.

GGD27 (IRAS 18162−2048) is a small reflection nebula containing six point-like infrared sources, interpreted as a small group of massive YSOs (Yamashita et al. 1987; Stecklum et al. 1997). The object GGD 27-ILL (Aspin et al. 1991) is the probable illuminating source of the nebula and might also power the bipolar outflow seen in CO (Yamashita et al. 1995). The emission lines observed with ISO appear dominated by PDR emission rather than trace a shock driven by the outflow. The ISO emission-line spectrum is also indicative of a PDR origin, although the H_2 temperature falls outside the range predicted by the PDR models.

LkHα 225 (IRAS 20187+4111) is an embedded source in the BD+40°4124 region. The source was shown to be a triple system oriented north-south by Aspin et al. (1994). It is associated with a H_2O maser source and drives a CO outflow (Palla et al. 1994). The detection of [S I] emission shows that a shock must be present in the region. Van den Ancker et al. (2000a) studied the ISO spectra of LkHα 225 in more detail and concluded that the emission line spectrum can be well explained as arising in the combination of a C-shock produced by a slow ($\approx$ 20 km s^{-1}) outflow and a J-shock. In addition to this, we found absorption due to solid water ice and to gas-phase H_2O, CO and CO_2 in the line of sight towards LkHα 225, with unusually high gas/solid ratios. The extreme [O I]/[C II] ratio found at the position of LkHα 225 suggest that a PDR might be present throughout the region as well.

S106 IRS4 (IRAS 20255+3712) is a massive young stellar object believed to be the powering source for the well-known bipolar nebula S106. Apart from the central source IRS4 (Gehrz et al. 1982), S106 also contains an embedded cluster of about 160 stars, as well as an expanding ring of molecular material (Hodapp & Rayner 1991; Loushin et al. 1990; Staude & Elsässer 1993). Van den Ancker et al. (2000b) made a more detailed study of the ISO SWS and LWS spectra of S106 and concluded that the emission line spectrum could be well explained as arising from the superposition of an extended H II region with a density of about 10^3 cm^{-3} surrounding an O6–8 star, and a PDR of much higher density (10^5–10^6 cm^{-3}). Since it is implausible that such densities would exist throughout the PDR, the PDR must be clumpy in nature.

AFGL 2591 (IRAS 20275+4001) is one of the rare examples of a relatively isolated massive young star. Located in the obscured Cygnus X region, it is invisible in the optical, although it is one of the brightest YSOs at infrared to submm wavelengths. It is associated with a powerful bipolar molecular outflow (Lada et al. 1984) and is surrounded by an envelope of which part might be in free fall collapse onto the star (van der Tak et al. 1999). Tamura & Yamashita (1992) discovered a bipolar outflow-like structure extending over 90$''$ in ro-vibrational H_2 emission, suggesting a shock origin for the spectral lines detected with ISO. This would also explain the absence of PAH emission. The [O I]/[C II] flux ratio is more suggestive of a PDR origin, though.

Cep A East (IRAS 22543+6145) is the eastern lobe of an energetic, complex molecular outflow (Bally & Lane 1982), believed to be powered by the deeply embedded source HW-2 only visible at radio wavelengths (Hughes & Wouterloot 1984). Cep A East is the site of a fast jet, as well as a number of Herbig-Haro like objects, whereas the western lobe of the Cep A outflow contains a number of distinct shells (Hartigan et al. 1996; Goetz et al. 1998). ISO SWS observations of the western lobe were discussed by Wright et al. (1996), who modelled the emission line spectrum as the combination of several C-type shocks with a planar J-shock of 70–80 km s^{-1}. Van den Ancker et al. (2000b) discussed the entire SWS and LWS spectra of Cep A East in detail and concluded that the continuum radiation at near-infrared wavelengths is dominated by emission from the embedded source IRS 6A (Casement & McLean 1996), whereas another, more luminous, component only becomes visible in the far-infrared. We explain the infrared emission line spectrum as the superposition of a 20 km s^{-1} C-shock and a 60 km s^{-1} J-shock arising in a dense (10^6 cm^{-3}) medium.

Elias 3-1 (IRAS 04155+2812) is an embedded luminous object which is believed to be a young Herbig Ae star. It illuminates a cometary-shaped reflection nebula, in which an east-west oriented elongated structure is visible at near-infrared wavelengths, interpreted by Haas et al. (1997) as two lobes of a cone-like structure. One feature that distinguishes Elias 3-1 is that it is one of the only three sources known that shows the 3.43 and 3.53 μm infrared emission bands, as well as the other infrared emission features usually attributed to PAHs (Schutte et al. 1990). No infrared emission lines were detected.

T Tau (IRAS 04190+1924) is a young binary system, consisting of an optically visible K0–1e classical T Tauri star with an embedded (A_V = 17$^{\rm m}$4), more luminous, companion. Both stars are surrounded by a compact nebula as well as spatially separated arc-shaped cloud 30$''$ to the west. The ISO SWS observations presented here only include the compact nebula, whereas the LWS observations also include the more extended cloud. Both the optically visible and embedded components of the T Tau system drive separate molecular outflows, whereas the embedded source might also power a string of Herbig-Haro objects as far away as 38 arcminutes (1.55 pc) from the source (Edwards & Snell 1982; van Langevelde et al. 1994; Reipurth et al. 1997). Van den Ancker et al. (1999) and Spinoglio et al. (2000) studied the complete ISO SWS and LWS spectra of T Tau in more detail and came to the conclusion that the observed molecular and atomic fine structure emission line spectrum can be well explained as arising in the superposition of a C-shock with a speed of $\approx$ 35 km s^{-1} and a much faster ($\approx$ 100 km s^{-1}) J-shock arising in a fairly dense (5 $\times$ 10^4 cm^{-3}) medium.

HD 97048 (IRAS 11066−7722) is a fairly typical late B-type Herbig Ae/Be star located in the Chamaeleon I dark cloud. Wesselius et al. (1984) discovered the source to have a strong infrared excess, which was interpreted in terms of a flattened shell or disk of dust particles heated by the central star by Thé et al. (1986). One feature that distinguishes HD 97048 is that it is one of the only three sources known that shows the 3.43 and 3.53 μm infrared emission bands, as well as the other infrared emission features usually attributed to PAHs (Schutte et al. 1990). Although extended mid-infrared emission around HD 97048 has been reported from multi-aperture photometry (Prusti et al. 1994), unpublished N band imaging by the authors with the TIMMI instrument at the ESO 3.6 m telescope show the source to be point-like (diameter $< 1''$), suggesting that the extended emission might be limited to the PAH bands. Only weak [O I] and [C II] emission was detected. If we assume that this emission comes from the same region as the continuum emission, it is compatible with an origin in the surface layer of a circumstellar disk surrounding HD 97048, acting as a PDR.

HD 97300 (IRAS 11082−7620) is a B9 star located in the Cha I complex. The absence of Hα emission and infrared excess at wavelengths shortwards of 5 μm suggests that it is a relatively evolved object within the group of Herbig Ae/Be stars (Thé et al. 1986). HD 97300 is located near (or is seen projected on) the reflection nebula Ced 112, in which Siebenmorgen et al. (1998) discovered a ring of PAHs with ISOCAM. No emission lines were detected with SWS.

HR 5999 (IRAS 16052−3858) is one of the best studied Herbig Ae stars. In the visual, it shows irregular large-amplitude photometric variations due to variable amounts of circumstellar extinction (Tjin A Djie et al. 1989; Thé et al. 1996). HR 5999 is located in the pre-main sequence instability strip, and also shows regular pulsations similar to those observed in the evolved δ Scuti stars (Kurtz & Marang 1995; Marconi & Palla 1998). In the infrared, HR 5999 is a fairly isolated point source (Siebenmorgen et al. 1997), suggesting the star has cleared most of its wide stellar environment. This is in agreement with the non-detection of infrared emission lines with ISO.

R CrA is a well studied Herbig Ae star at the apex of a cometary nebula in the Corona Australis cloud. In the visual, it shows strong photometric variations, while its visual absorption line spectrum is also variable, suggesting it may in fact be a composite system (Bibo et al. 1992; van den Ancker et al. 1998). Several strong molecular outflows containing knots of shocked gas have been detected in the vicinity of R CrA, but recent high-resolution continuum and molecular mappings of the region have shown that the driving sources of these are the embedded sources IRS7 and HH100-IR rather than the optical Herbig stars in the region (Harju et al. 1993; Anderson et al. 1997). The detection of [S I] shows that a shock must be present within the SWS beam. Most likely, this is due to the outflow of IRS7.

T CrA is a late-type Herbig star located in the tail of a cometary nebula in the Corona Australis cloud. It shows strong photometric variations in the visual, probably due to variable amounts of circumstellar extinction (Bibo et al. 1992). Based on optical spectro-astrometric measurements, Bailey (1998) suggested T CrA to be a binary system. Ward-Thompson et al. (1987) reported the presence of a jet associated with T CrA, but more recent papers suggest that this may in fact be part of the east-west molecular outflow from the source IRS7 in the region around R CrA (Canto et al. 1986; Harju et al. 1993; Anderson et al. 1997). The H_2 emission detected by ISO is suggestive of a C-shock which may be attributed to this same outflow.

WW Vul (IRAS 19238+2106) is a prototypical Herbig Ae star showing large amplitude photometric variations due to variable circumstellar extinction (Friedemann et al. 1993), as well as evidence for the presence of evaporating solid bodies (Grinin et al. 1996). It shows a large infrared excess, indicative of the presence of a dusty circumstellar disk or envelope. WW Vul is located in relative isolation, which is confirmed by our non-detection of infrared emission lines.

BD+40°4124 (V1685 Cyg) is the most massive member of a small cluster of young stars, commonly known as the BD+40°4124 group (Hillenbrand et al. 1992). It is the ionizing source of a low-density ($\approx 10^2$ cm^{-3}) H II region, surrounded by a dense ($> 10^5$ cm^{-3}) PDR (van den Ancker et al. 2000a). The lines detected with ISO are indicative of PDR emission. In view of the luminosity of BD+40°4124 and the strong [C II] emission detected at the position of LkHα 225, it seems likely that the PDR is more extended than the ISO beam and may in fact produce observable PDR emission lines throughout the optical reflection nebula.

LkHα 224 (V1686 Cyg) is a fairly typical Herbig Ae star located in the BD+40°4124 region. In the optical it shows large variations in brightness due to variable amounts of circumstellar extinction (Wenzel 1980; Shevchenko et al. 1991). One remarkable aspect about LkHα 224 is the complete absence of a 10 μm silicate feature, either in absorption or emission in its spectrum (van den Ancker et al. 2000a). These authors also studied the infrared emission line spectrum of LkHα 224 and concluded that it is most likely due to non-dissociative shock produced by a slow (≈ 20 km s^{-1}) outflow arising from LkHα 225.

HD 200775 is the illuminating star of the well-known reflection nebula NGC 7023 (IRAS 20599+6755). A biconical cavity of $\approx 20''$ diameter surrounds the star, outside of which the nebulosity shows a highly filamentary structure (Rogers et al. 1995; Lemaire et al. 1996; Gerin et al. 1998). Observations with ISOCAM and ISOPHOT revealed the nebulosity to show strong emission bands due to Polycyclic Aromatic Hydrocarbons (Cesarsky et al. 1996; Laureijs et al. 1996). The SWS observations shortward of 12.0 μm only include the central star and the cavity, whereas the SWS data at longer wavelengths as well as the LWS spectrum also cover part of the PDR. The [O I]/[C II] ratio clearly reflects this PDR nature. Fuente et al. (2000) have analyzed ISO SWS observations centered on other parts of NGC 7023 and concluded that they arise in a PDR with temperatures in the range 300–700 K, and with an ortho/para ratio of H_2 of 1.5–2. Our observations suggest the PDR to have a density of $\approx 10^5$ cm^{-3}, much higher than the modelling results of the NGC 7023 PDR by Chokshi et al. (1988). Most likely the lines we have detected are dominated by a few of the high density clumps reported by Martini et al. (1997).

7. Discussion and conclusions

In the previous sections we have seen that based on the observed H_2 and atomic fine-structure lines we can make a distinction between PDRs and shocks with relative ease, and derive the physical properties in the emitting region, provided that key lines like [S I], [O I] and [C II] and the low-lying pure rotational molecular hydrogen lines were detected. The mere presence of [S I] is a sure way to recognize a shock, whereas the [O I] 63.2 μm/[C II] 157.7 μm ratio is able to distinguish PDRs of average to high density from shocks. From Table 6 we note that both shocks and PDRs are observed near Class I YSOs, whereas Class II YSOs only produce PDR emission. Note that the three Class II sources in whose vicinity we have detected [S I] emission, T Tau, LkHα 224 and R CrA, are all located near Class I sources driving a strong bipolar outflow. We associate the observed [S I] emission in these three sources with the embedded instead of the optical star.

An interesting question which we have not yet addressed in the previous sections is whether the heating efficiency assumed in the theoretical models is confirmed by the observations presented here. This efficiency will determine the absolute line fluxes, and could also influence the detailed structure of PDRs and shocks. For PDRs, the model parameter which determines the efficiency is the ratio of gas heating to the far-ultraviolet absorption rate of dust grains and PAHs, ε. On theoretical grounds, it is expected that the maximum allowed value of ε would be 3–5% (Bakes & Tielens 1994). This efficiency decreases when the PAHs are charged up and hence decreases with increasing G (ionization rate) and decreasing n_e (recombination rate; Bakes & Tielens 1998). Since for most sources in our sample the lines which we have detected include the major PDR coolants [O I] 63.2 μm, [C II] 158 μm and [Si II] 34.8 μm we are able to directly derive a value of ε for our PDR sources. For this reason, we have plotted the summed intensity in all detected lines against the values of G derived from the infrared continuum flux derived listed in Table 6. From this plot (Fig. 7), in which we also show lines of constant ε, it can be seen that most of our PDR

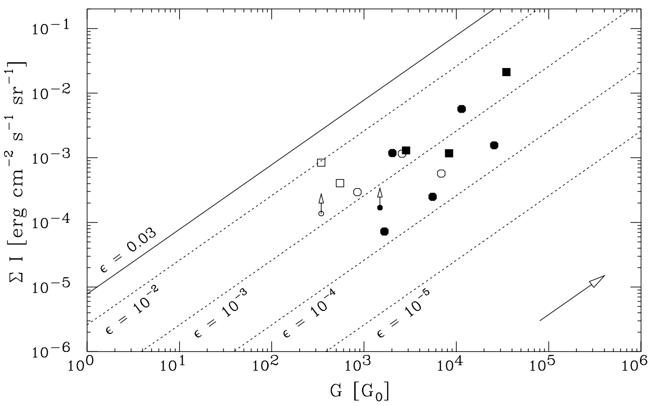

Fig. 7. Comparison of the sum the fluxes of all observed lines with G values as derived from the infrared continuum flux. Plots symbols have the same meaning as in Fig. 3. Lower limits are shown for objects in which one or two of the major coolants ([O I] 63 μm, [C II] 158 μm, [Si II] 35 μm) were not observed. Also shown are lines of equal ε (ratio of gas heating to far-ultraviolet absorption rate of grains and PAHs).

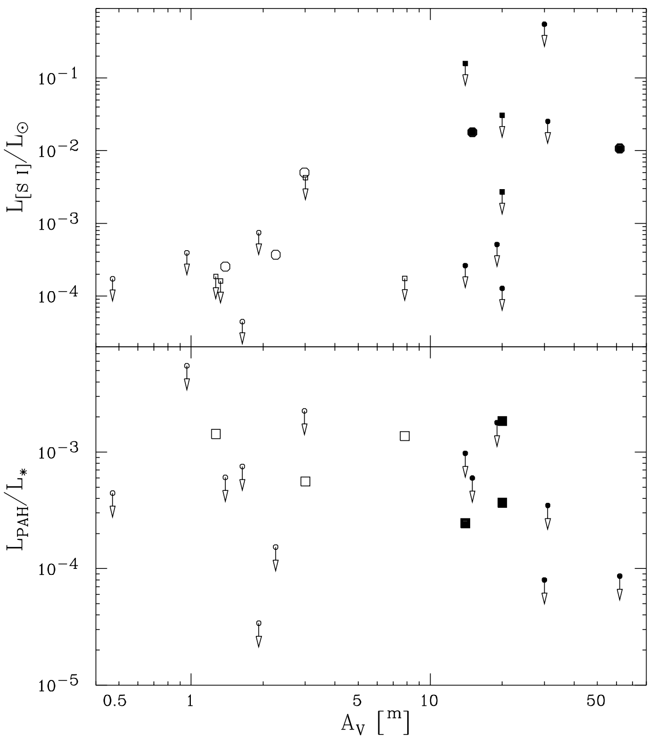

Fig. 8. Comparison of flux emitted in [S I] 25.3 μm (top) and 6.2 μm PAH band (bottom) with estimated visual extinction towards the associated source. Plot symbols have the same meaning as in Figs. 3–6.

sources (as identified from the associated PAH emission) have ε of a few times 10^{-3}. This estimate is nearly independent of the beam filling factor. Although somewhat lower than assumed in most PDR models, this value agrees well with those observed towards PDRs in different astrophysical environments (see e.g. Hollenbach & Tielens 1999).

As a final note, let us now wonder how to put our main result, that both shocks and PDRs are observed near Class I YSOs, whereas Class II YSOs only show PDR emission, in context. In the previous sections we have seen that the detection of [S I], indicative of shocks, and PAH-emission, indicative of PDR activity, appear mutually exclusive. To illustrate this mutual exclusion of [S I] and the PAH emission and to illustrate its dependence on the evolutionary state of the YSO, we have created plots of the luminosity in the [S I] 25.3 μm line and in the 6.2 μm PAH band, normalized to the bolometric luminosity, against the visual extinction A_V for the sources in our sample (Fig. 8). We can see here that the Class I sources for which we have detected [S I] emission, LkHα 225 and Cep A East, are also among the sources with higher values of A_V. However, apparently the mere embeddedness of a source does not guarantee that strong [S I] is present, as evidenced by some of the upper limits plotted in Fig. 8.

PAH emission was observed in both Class I (IRAS 03260+3111, GGD 27-ILL, S106 IRS4) and Class II (BD+40°4124, HD 97048) sources. The range in fraction of the total luminosity coming out in the 6.2 μm C–C stretch mode does not appear different between the two groups, although the cooler stars in both groups appear to have a higher $L_{\rm PAH}/L_{\rm bol}$ than the hotter stars. The values of A_V used in Fig. 8 are those for the associated continuum source; the lines do not necessarily have to suffer from the same amount of extinction. Because a young star is expected to clear its circumstellar environment as it accretes mass, these values of A_V may be taken as a rough indication of evolutionary status. Geometry is however also important in interpreting these results as exemplified by S106 IRS4 where our direct view of the YSO is inhibited by an optically thick circumstellar disk but the gas along the poles is photoionized by the star (van den Ancker et al. 2000b).

It is interesting that the most embedded source in our sample, Cep A East, also has the highest [S I] luminosity, and that all Class I sources which show PAH emission are only moderately embedded. This is exactly what one would also expect: as a star has just formed, it is heavily embedded and any PAH emission arising in a PDR close to the star will be completely obscured. As long as the young star accretes matter it will also drive a bipolar outflow, which can power a shock as it interacts with the ambient medium. As this process proceeds, the surroundings of the star are cleared and the UV radiation from the newly formed star can escape to illuminate a PDR. The intensity of the PDR emission is mainly determined by its spatial extent. As the material in the wide circumstellar environment is slowly cleared by the still strong stellar wind and the effect of photoevaporation, the extent of the PDR and hence the intensity of the PDR lines will gradually decrease until the only, weak, source of PDR emission will become the surface of a circumstellar disk, acting as a PDR (e.g. the case of HD 97048). With the tools presented in this paper, the study of such PDRs offers the promise of a fundamental better understanding of the processes occurring in protoplanetary disks when far-infrared spectrographs with higher spatial resolution become available.

Acknowledgements. The authors would like to thank the SWS and LWS IDTs for their help with the observations. Drs. David Hollenbach and Michael Kaufman are gratefully acknowledged for shocking discussions. MvdA acknowledges financial support from NWO grant 614.41.003 and through a NWO *Pionier* grant to L.B.F.M. Waters. This research has made use of the Simbad data base, operated at CDS, Strasbourg, France.

References

Anderson, I.M., Harju, J., Knee, L.B.G., Haikala, L.K. 1997, A&A 321, 575
Aspin, C., Rayner, J.T., McLean, I.S., Hayashi, S.S. 1990, MNRAS 246, 565
Aspin, C., Sandell, G., Weintraub, D.A. 1994, A&A 282, L25
Bailey, J. 1998, MNRAS 301, 161
Bakes, E.L.O., Tielens, A.G.G.M. 1994, ApJ 427, 822
Bakes, E.L.O., Tielens, A.G.G.M. 1998, ApJ 499, 258
Bally, J., Lane, A.J. 1982, ApJ 257, 612
Bibo, E.A., Thé, P.S., Dawanas, D.N. 1992, A&A 260, 293
Black, F.H., van Dishoeck. E.F. 1987, ApJ 322, 412
Brand, P.W.J.L., Moorhouse, A., Burton, M.G., Geballe, T.R., Bird, M., Wade, R. 1988, ApJ 334, L103
Burton, M.R., Geballe, T.R., Brand, P.W.J.L., Webster, A.S. 1988, MNRAS 231, 617
Burton, M.R., Brand, P.W.J.L., Geballe, T.R., Webster, A.S. 1989, MNRAS 236, 409
Burton, M.R., Geballe, T.R., Brand, P.W.J.L., Moorhouse, A. 1990a, ApJ 352, 625
Burton, M.R., Hollenbach, D.J., Haas, M.R., Erickson, E.F. 1990b, ApJ 355, 197
Burton, M.G., Hollenbach, D.J., Tielens, A.G.G.M. 1992a, ApJ 399, 563
Burton, M.G., Bulmer, M., Moorhouse, A., Geballe, T.R., Brand, P.W.J.L. 1992b, MNRAS 257, 1p
Canto, J., Sarmiento, A., Rodríguez, L.F. 1986, Rev. Mex. Astron. Astrofis. 13, 107
Carr, J.S. 1990, AJ 100, 1244
Casement, L.S., McLean, I.S. 1996, ApJ 462, 797
Cesarsky, D., Cox, P., Pineau des Forêts, G., van Dishoeck, E.F., Boulanger, F., Wright, C.M. 1999, A&A 348, 945
Cesarsky, D., Lequeux, J., Abergel, A., Perault, M., Palazzi, E., Madden, S., Tran D. 1996, A&A 315, L305
Chernoff, D.F., Hollenbach, D.J., McKee, C.F. 1982, ApJ 259, L97
Chokshi, A., Tielens, A.G.G.M., Werner, M.W., Castelaz, M.W. 1988, ApJ 334, 803
Clegg, P.E., Ade, P.A.R., Armand, C., et al., 1996, A&A 315, L38
Crampton, D., Fisher, W.A. 1974, Pub. Dom. Astrophys. Obs. 14, 283
Crawford, M.K., Lugten, J.B., Fitelson, W., Genzel, R., Melnick, G. 1986, ApJ 303, L57
Dabrowski, I. 1984, Canadian J. Phys. 62, 1639
Dame, T.M., Thaddeus, P. 1985, ApJ 297, 751
Davis, C.J., Moriarty-Schieven, G., Eislöffel, J., Hoare, M.G., Ray, T.P. 1998, AJ 115, 1118
Davis, C.J., Mundt, R., Eislöffel, J., Ray, T.P. 1995, AJ 110, 766
de Graauw, Th., Haser, L.N., Beintema, D.A., et al., 1996, A&A 315, L49
Draine, B.T., Bertoldi, F. 1996, ApJ 468, 269
Edwards, S., Snell, R.L. 1982, ApJ 261, 151
Emery, R., Aannestad, P., Minchin, N., et al., 1996, A&A 315, L285
Finkenzeller, U., Mundt, R., 1984, A&AS 55, 109
Fluks, M.A., Plez, B., Thé, P.S., de Winter, D., Westerlund, B.E., Steenman, H.C. 1994, A&AS 105, 311
Friedemann, C., Reimann, H.G., Gürtler, J, Tóth, V. 1993, A&A 277, 184
Fuente, A., Martín-Pintado, J., Rodríguez-Fernández, N.J., Rodríguez-Franco, A., de Vicente, P., Kunze, D. 2000, A&A 354, 1053
Gehrz, R.D., Grasdalen, G.L., Castelaz, M., Gullixson, C., Mozurkewich, D., Hackwell, J.A. 1982, ApJ 254, 550
Gerin, M., Phillips, T.G., Keene, J., Betz, A.L., Boreiko, R.T. 1998, ApJ 500, 329
Goetz, J.A., Pipher, J.L., Forrest, W.J., et al., 1998, ApJ 504, 359
Gómez, M., Whitney, B.A., Kenyon, S.J. 1997, AJ 114, 1138
Gray, R.O., Corbally, C.J. 1998, AJ 116, 2530
Grinin, V.P., Kozlova, O.V., Thé, P.S., Rostopchina, A.N. 1996, A&A 309, 470
Haas, M.R., Hollenbach, D.J., Erickson, E.F. 1986, ApJ 301, L57
Haas, M.R., Hollenbach, D.J., Erickson, E.F. 1991, ApJ 374, 555
Haas, M.R. 1997, personal communication
Haas, M.R., Leinert, C., Lenzen, R. 1992, A&A 261, 130
Haas, M.R., Leinert, C., Richichi, A. 1997, A&A 326, 1076
Habing, H.J. 1968, Bull. Astron. Inst. Netherlands 19, 421
Harju, J., Haikala, L.K., Mattila, K., Mauersberger, R., Booth, R.S., Nordh, H.L. 1993, A&A 278, 569
Hartigan, P., Carpenter, J.M., Dougados, C., Skrutskie, M.F. 1996, AJ 111, 1278
Harvey, P.M., Campbell, M.F., Hoffmann, W.F., Thronson, H.A., Gatley, I. 1979, ApJ 229, 990
Hasegawa, T., Gatley, I., Garden, R.P., Brand, P.W.J.L., Ohishi, M., Hayashi, M., Kaifu, N. 1987, ApJ 318, L77
Hayashi, M., Hasegawa, T., Gatley, I., Garden, R.P., Kaifu, N. 1985, MNRAS 215, 31p
Herbig, G.H., Jones, B.F. 1983, AJ 88, 1040
Hillenbrand, L.A., Strom, S.E., Vrba, F.J., Keene, J. 1992, ApJ 397, 613
Hillenbrand, L.A., Meyer, M.R., Strom, S.E., Skrutskie, M.F. 1995, AJ 109, 280
Hodapp, K.W., Rayner, J. 1991, AJ 102, 1108
Hogerheijde, M.R., van Dishoeck, E.F., Blake, G.A., van Langevelde, H.J. 1998, ApJ 502, 315
Hollenbach, D.J., McKee, C.F. 1989, ApJ 342, 306
Hollenbach, D.J., Tielens, A.G.G.M. 1999, Rev. Mod Phys. 71, 173
Hughes, J.D., Hartigan, P., Graham, J.A., Emerson, J.P., Marang, F. 1991, AJ 101, 1013
Hughes, V.A., Wouterloot, J.G.A. 1984, ApJ 276, 204
Jaffe, D.T., Genzel, R., Harris, A.I., Howe, J.E., Stacey, G.J., Stutzki, J. 1990, ApJ 353, 193
Kaufman, M.J., Neufeld, D.A. 1996, ApJ 456, 611
Keene, J., Masson, C.R. 1990, ApJ 355, 635
Kenyon, S.J., Brown, D.I., Tout, C.A., Berlind, P. 1998, AJ 115, 2491
Kenyon, S.J., Dobrzycka, D., Hartmann, L. 1994, AJ 108, 1872
Kenyon, S.J., Hartmann, L. 1995, ApJS 101, 117
Kessler, M.F., Steinz, J.A., Anderegg, M.E., et al., 1996, A&A 315, L27
Knee, L.B.G. 1992, A&A 259, 283
Kraemer, K.E., Jackson, J.M., Lane, A.P. 1998, ApJ 503, 785
Kurtz, D.W., Marang, F. 1995, MNRAS 276, 191
Kurucz, R.L. 1991, in *"Stellar atmospheres–Beyond classical models"* (eds. A.G. Davis Philip, A.R. Upgren, K.A. Janes), L. Davis press, Schenectady, New York, p. 441
Lada, C.J., Harvey, P.N. 1981, ApJ 245, 58
Lada, C.J., Thronson, H.A., Smith, H.A., Schwarz, P.R., Glaccum, W. 1984, ApJ 286, 302
Laureijs, R.J., Acosta-Pulido, J., Abraham, P., Kinkel, U., Klaas, U., Castaneda, H.O., Cornwall, L., Gabriel, C., Heinrichsen, I., Lemke, D., Pelz G., Schulz B., Walker, H.J. 1996, A&A 315, L313

Leech, K., et al., 1997, *"SWS Instrument Data Users Manual"*, Issue 3.1, SAI/95-221/Dc
Leibowitz, E.M., Danziger, I.J. 1983, MNRAS 204, 273
Lemaire, J.L., Field, D., Gerin, M., Leach, S., Pineau des Forêts, G., Rostas, F., Rouan, D. 1996, A&A 308, 895
Liseau, R., White, G.J., Larsson, B., et al., 1999, A&A 344, 342
Loushin, R., Crutcher, R.M., Bieging, J.H. 1990, ApJ 362, L67
Magnier, E.A., Volp, A.W., Laan, K., van den Ancker, M.E., Waters, L.B.F.M. 1999, A&A 352, 228
Marconi, A., Testi, L., Natta, A., Walmsley, C.M. 1998, A&A 330, 696
Marconi, M., Palla, F. 1998, ApJ 507, L141
Marraco, H.G., Rydgren, A.E. 1981, AJ 86, 62
Martini, P., Sellgren, K., Hora, J.L. 1997, ApJ 484, 296
Mel'nikov, S.Y., Shevchenko, V.S., Grankin, K.N. 1995, Astron. Rep. 39, 42
Minchin, N.R., Hough, J.H., Burton, M.G., Yamashita, T. 1991, MNRAS 251, 522
Moriarty-Schieven, G.H., Wannier, P.G., Tamura, M., Keene, J. 1992, ApJ 400, 260
Mundt, R., Ray, T.P., Raga, A.C. 1991, A&A 252, 740
Myers, P.C., Heyer, M., Snell, R.L., Goldsmith, P.F. 1988, ApJ 324, 907
Neufeld, D.A., Melnick, G.J., Harwitt, M. 1998, ApJ 506, L75
Oliva, E., Moorwood, A.F.M., Danziger, I.J. 1990, A&A 240, 453
Oliva, E., Lutz, D., Drapatz, S., Moorwood, A.F.M. 1999a, A&A 341, L75
Oliva, E., Moorwood, A.F.M., Drapatz, S., Lutz, D., Sturm, E. 1999b, A&A 343, 943
Padgett, D.L., Brandner, W., Stapelfeldt, K.R., Strom, S.E., Terebey, S., Koerner, D. 1999, AJ 117, 1490
Palla, F., Stahler, S.W. 1993, ApJ 418, 414
Palla, F., Testi, L., Hunter, T.R., Taylor, G.B., Prusti, T., Felli, M., Natta, A., Stanga, R.M. 1995, A&A 293, 521
Parmar, P.S., Lacy, J.H., Achtermann, J.M. 1991, ApJ 372, L25
Parmar, P.S., Lacy, J.H., Achtermann, J.M. 1994, ApJ 430, 786
Poglitsch, A., Herrmann, F., Genzel, R., Madden, S.C., Nikola, T., Timmermann, R., Geis, N., Stacey, G.J. 1996, ApJ 462, L43
Prusti, T., Natta, A., Palla, F. 1994, A&A 292, 593
Rayner, J. 1994, in *"Infrared Astronomy with Arrays: The next generation"*, ed. I.S. McLean (Dordrecht: Kluwer), p. 185
Reipurth, B., Bally, J., Devine, D. 1997, AJ 114, 2708
Richter, M.J., Graham, J.R., Wright, G.S. 1995a, ApJ 454, 277
Richter, M.J., Graham, J.R., Wright, G.S., Kelly, D.M., Lacy, J.H. 1995b, ApJ 449, L83
Rodríguez, L.F., Moran, J.M., Ho, P.T.P., Gottlieb, E.W. 1980, ApJ 235, 845
Rogers, C., Heyer, M.H., Dewdney, P.E. 1995, ApJ 442, 694
Rosenthal, D., Bertoldi, F., Drapatz, S. 2000, A&A 356, 705
Rydgren, A.E. 1980, AJ 85, 444
Schutte, W.A., Tielens, A.G.G.M., Allamandola, L.J., Cohen, M., Wooden, D.H. 1990, ApJ 360, 577
Shevchenko, V.S., Ibragimov, M.A., Chernysheva, T.L. 1991, Astron. Zh. 68, 466 (SvA 35, 229)
Siebenmorgen, R., Prusti, T., Krügel, E., Natta, A. 1997, in proc. *"First ISO Workshop on Analytical Spectroscopy"*, eds. A.M. Heras et al., ESA SP-419, p. 229
Siebenmorgen, R., Natta, A., Krügel, E., Prusti, T. 1998, A&A 339, 134
Snell, R.L., Loren, R.B., Plambeck, R.L. 1980, ApJ 239, L17
Snell, R.L., Scoville, N.Z., Sanders, D.B., Erickson, N.R. 1984, ApJ 284, 176
Spinoglio, L., Giannini, T., Nisini, B., et al., 2000, A&A 353, 1055
Stacey, G.J., Jaffe, D.T., Geis, N., Genzel, R., Harris, A.L., Poglitsch, A., Stutzki, J., Townes, C.H. 1993, ApJ 404, 219
Staude, H.J., Elsässer, H. 1993, A&A Rev. 5, 165
Stecklum, B., Feldt, M., Richichi, A., Calamai, G., Lagage, P.O. 1997, ApJ 479, 339
Steiman-Cameron, T.Y., Haas, M.R., Tielens, A.G.G.M., Burton, M.G. 1997, ApJ 478, 261
Tamura, M., Yamashita, T. 1992, ApJ 391, 710
Terebey, S., Vogel, S.N., Myers, P.C. 1989, ApJ 340, 472
Thé, P.S., Pérez, M.R., Voshchinnikov, N.V., van den Ancker, M.E. 1996, A&A 314, 233
Thé, P.S., Wesselius, P.R., Tjin A Djie, H.R.E., Steenman, H. 1986, A&A 155, 347
Tielens, A.G.G.M., Hollenbach, D.J. 1985, ApJ 291, 722
Timmermann, R., Bertoldi, F., Wright, C.M., Drapatz, S., Draine, B.T., Haser, L., Sternberg, A. 1996, A&A 315, L281
Tjin A Djie, H.R.E., Thé, P.S., Andersen, J., Nordstrom, B., Finkenzeller, U., Jankovics, I. 1989, A&AS 78, 1
Trams, N., et al., 1997, *"ISO-LWS Instrument Data Users Manual"*, Issue 5.0, SAI/95-219/Dc
Turner, J., Kirby-Docken, K., Dalgarno, A. 1977, ApJS 35, 281
van den Ancker, M.E., Thé, P.S., Tjin A Djie, H.R.E., Catala, C., de Winter, D., Blondel, P.F.C., Waters, L.B.F.M. 1997, A&A 324, L33
van den Ancker, M.E., de Winter, D., Tjin A Djie, H.R.E. 1998, A&A 330, 145
van den Ancker, M.E., Wesselius, P.R., Tielens, A.G.G.M., van Dishoeck, E.F., Spinoglio, L. 1999, A&A 348, 877
van den Ancker, M.E., Wesselius, P.R., Tielens, A.G.G.M. 2000a, A&A 355, 194
van den Ancker, M.E., Tielens, A.G.G.M., Wesselius, P.R. 2000b, A&A 358, 1035
van der Tak, F.F.S., van Dishoeck, E.F., Evans, N.J., Bakker, E.J., Blake, G.A. 1999, ApJ 522, 991
van Dishoeck, E.F., Jansen, D.J., Phillips, T.G. 1993, A&A 279, 541
van Langevelde, H.J., van Dishoeck, E.F., Blake, G.A. 1994, ApJ 425, L45
Voshchinnikov, N.V. 1981, Astron. Tsirk. 1200, 1
Ward-Thompson, D., Warren-Smith, R.F., Scarrott, S.M., Wolstencroft, R.D. 1985, MNRAS 215, 537
Warren, W.H., Hesser, J.E. 1978, ApJS 36, 497
Wenzel, W. 1980, Mitt. Ver. Sterne 8, 182
Wesselius, P.R., Beintema, D., Olnon, F.M. 1984, ApJ 278, L37
Whittet, D.C.B., Kirrane, T.M., Kilkenny, D., Oates, A.P., Watson, F.G., King, D.J. 1987, MNRAS 224, 497
Whittet, D.C.B., Prusti, T., Franco, G.A.P., Gerakines, P.A., Kilkenny, D., Larson, K.A., Wesselius, P.R. 1997, A&A 327, 1094
Wright, C.M., Drapatz, S., Timmermann, R., van der Werf, P.P., Katterloher, R., de Graauw, Th. 1996, A&A 315, L301
Yamashita, T., Sato, S., Suzuki, S., Hough, H.J., McLean, I., Garden, R., Gatley, I. 1987, A&A 177, 258
Yamashita, T., Murata, Y., Kawabe, R., Kaifu, N., Tamura, M. 1991, ApJ 373, 560
Yamashita, T., Tamura, M. 1992, ApJ 387, L93
Zinnecker, H., Preibisch, Th. 1994, A&A 292, 152